Naval Research Laboratory

Washington, DC 20375-5320

NRL/MR/6410--95-7662

An Analysis of Gas Phase Ethanol/Water Chemistry for Diamond CVD

ROBERT S. SINKOVITS

Center for Reactive Flow and Dynamical Systems
Laboratory for Computational Physics and Fluid Dynamics

C. RICHARD DEVORE

Center for Computational Physics Developments
Laboratory for Computational Physics and Fluid Dynamics

VASGEN A. SHAMAMIIA

Chemistry Dynamics and Diagnos
Chemistry Division

CHARLES K. WESTBROOK

Lawrence Livermore National Laboratory
Livermore, California

March 29, 1995

REPORT DOCUMENTATION PAGE

Form Approved
OMB No. 0704-0188

1. AGENCY USE ONLY (*Leave Blank*)	2. REPORT DATE	3. REPORT TYPE AND DATES COVERED
	March 29, 1995	

4. TITLE AND SUBTITLE

An Analysis of Gas Phase Ethanol/Water Chemistry for Diamond CVD

5. FUNDING NUMBERS

PE -62712E

6. AUTHOR(S)

Robert S. Sinkovits, Richard C. DeVore, Vasgen A. Shamamian, and Charles K. Westbrook*

7. PERFORMING ORGANIZATION NAME(S) AND ADDRESS(ES)

Naval Research Laboratory
Washington, DC 20375-5320

Lawrence Livermore Nat'l Lab
Livermore, CA 94550

8. PERFORMING ORGANIZATION REPORT NUMBER

NRL/MR/6410--95-7662

9. SPONSORING/MONITORING AGENCY NAME(S) AND ADDRESS(ES)

Advanced Research Projects Agency
3701 North Fairfax Drive
Arlington, VA 22203-1714

10. SPONSORING/MONITORING AGENCY REPORT NUMBER

11. SUPPLEMENTARY NOTES

*Lawrence Livermore National Laboratory
California 94550

12a. DISTRIBUTION/AVAILABILITY STATEMENT

Approved for public release; distribution unlimited.

12b. DISTRIBUTION CODE

13. ABSTRACT (*Maximum 200 words*)

Chemical kinetics calculations have been carried out on ethanol (EtOH)/water mixtures at a range of temperatures, pressures and EtOH/H_2O ratios. The results show that the mole fractions of many chemical species depend very sensitively on the initial EtOH/H_2O ratio and diverge sharply after an induction time which depends both on pressure and temperature. We explain this divergence primarily in terms of the stability of carbon monoxide and show that the rate-limiting steps that dictate the induction time are the molecular hydrogen dissociation reactions. Our calculations also predict the dependence of the concentrations of potential growth (C, CH_3, C_2H_2) and etching (O, OH, O_2) species for diamond chemical vapor deposition (CVD) on operating conditions.

14. SUBJECT TERMS

Ethanol/water chemistry
Diamond growth
Chemical vapor deposition
Chemical kinetics

15. NUMBER OF PAGES

46

16. PRICE CODE

17. SECURITY CLASSIFICATION OF REPORT	18. SECURITY CLASSIFICATION OF THIS PAGE	19. SECURITY CLASSIFICATION OF ABSTRACT	20. LIMITATION OF ABSTRACT
UNCLASSIFIED	UNCLASSIFIED	UNCLASSIFIED	UL

NSN 7540-01-280-5500

Standard Form 298 (Rev. 2-89)
Prescribed by ANSI Std 239-18
298-102

CONTENTS

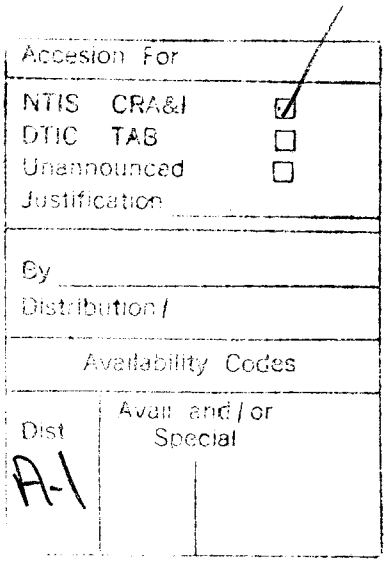

AN ANALYSIS OF GAS PHASE ETHANOL/WATER CHEMISTRY FOR DIAMOND CVD

I. INTRODUCTION

Diamond possesses unique physical properties which make it ideal for a number of technological applications including coatings for cutting tools, thermal spreaders for electronic devices, high-transmittance optical windows and high-performance semiconductors. Previously, most artificial diamond was produced by high-pressure, high-temperature techniques, but with the advent of chemical vapor deposition (CVD), this technique has become the dominant way to grow high-quality diamond films. (For a more detailed treatment of diamond CVD technology, see the review article by Celli and Butler [1]). Early diamond CVD reactors used gas mixtures such as CO/CO_2 [2] and CO/H_2 [3], while later generations of reactors relied on mixtures of hydrogen and a carbon source, typically methane. In recent years there has been a return to feedstocks containing oxygen.

An analysis of a large number of diamond CVD experiments by Bachmann *et al.* [4] shows that in nearly all reactors which were successful in growing diamond, the compositions of the feed gases fell within a well defined region of a C/H/O ternary diagram. Bachmann *et al.* define the following variables as the coordinates of their diagram:

$$X_{O:\Sigma} = [O]/([O] + [H]) \tag{1}$$

$$X_{H:\Sigma} = [H]/([H] + [C]) \tag{2}$$

$$X_{C:\Sigma} = [C]/([C] + [O]), \tag{3}$$

and show that the diamond growth region is roughly bracketed by the lines $X_{C:\Sigma} = 0.57$ and $X_{C:\Sigma} = 0.50$. Their survey suggests that it is not the specific inlet gases themselves that are important, but rather their overall C/H/O ratio.

The majority of the CVD reactors analyzed in ref. [4] use H_2 as an inlet gas. Although diamond films have been grown quite successfully using H_2 as a feedstock,

Manuscript approved February 23, 1995.

one of the serious drawbacks is the hazard of explosion associated with the storage and handling of H_2, as well as of the typical carbon sources CH_4 and C_2H_2. It would be advantageous to the CVD growth of diamond films to develop reactors which yield high growth rates and utilize more benign gases. Recent experiments have demonstrated growth from methanol [5], ethanol/water/hydrogen [6], and EtOH/water [7].

In this paper we focus on the thermodynamics and chemical kinetics of $EtOH/H_2O$ under conditions of constant pressure and temperature. Previous studies of C/H/O systems include equilibrium calculations of $EtOH/H_2O$ [8] and kinetic studies of $CH_4/O_2/H_2$ [9–12], $C_2H_2/O_2/H_2$ [12], and CH_3OH/H_2 [13]. The calculations that we perform are not for any specific CVD reactor design or heating mechanism, but should be valid in all cases where the neutral chemistry is dominant. This assumption is clearly not valid for growth techniques such as electron-cyclotron resonance (ECR) where the operating pressure is in the mTorr range and e^--impact is the dominant H_2 dissociation mechanism, but should be at least partially valid for most reactors operating at pressures greater than one Torr. Although it should be possible to grow diamond using a variety of different alcohols, we have restricted our attention to EtOH since $EtOH/H_2O$ is the simplest alcohol-water system where we are able to tune the parameter $X_{C:\Sigma}$ so as to sample a region of the ternary diagram [4] from "no growth", through "diamond growth", to "non-diamond carbon growth". Using a methanol/water mixture it is only possible to sample the region of the phase diagram below the "CO line" corresponding to $X_{C:\Sigma} \leq 0.5$. An additional advantage of using EtOH in our study is the availability of a reliable reaction set for EtOH combustion. We expect that the analysis of $EtOH/H_2O$ presented in this paper should be easily extended to other alcohol-water systems.

The remainder of this paper is organized as follows. In the next section we describe both the chemistry reaction set and the approach used to perform the chemical

kinetics calculations. The results are presented in section III with an emphasis on the sharp divergence in species concentrations with inlet composition, the dependence of the H/H_2 ratio on operating conditions, the CO/CO_2 equilibrium and the ratio of C_1 to C_2 species. Finally, in section IV we summarize the results.

II. MODEL

A. Chemistry reaction set

The results of the chemical kinetics calculations presented in this paper were obtained using a hybrid chemistry scheme constructed from the Miller-Melius acetylene combustion set (MM-C_2H_2) [14] and the Lawrence Livermore National Laboratory EtOH combustion set (LLNL-EtOH) [15]. Our hybrid chemistry scheme contains a total of 249 reversible elementary reactions involving 54 species. Both sets express the forward reaction rates in the Arrhenius form

$$k = AT^B e^{-E/RT}, \tag{4}$$

and include enhanced third-body and pressure fall-off reactions. The LLNL-EtOH set explicitly specifies the reverse rate Arrhenius coefficients while the MM-C_2H_2 set uses reverse reaction rates calculated from the equilibrium constants. Although it is generally considered unwise to tamper with reaction schemes that have been optimized for the study of a particular system, we feel we have taken great care in combining and drawing on the strengths of the two sets. The LLNL-EtOH scheme would appear to be the natural choice for this study since it does a very detailed treatment of EtOH chemistry, but EtOH combustion takes place at temperatures ($T \leq 2000$ K) lower than those used in many CVD reactors ($T \geq 3000$ K). Consequently, the chemistry of species such as C and C_2, which are typically only found at high temperatures, is not considered. (Thermodynamic equilibrium calculations of EtOH-rich, $EtOH/H_2O$ mixtures show that the mole fractions of C and C_2 do not exceed

1×10^{-10} for temperatures less than $\sim$ 2000 K at 0.001 atm. and $\sim$ 2500 K at 1.0 atm.) The MM-C_2H_2 set on the other hand, which adequately describes the high-temperature chemistry of these carbon species, contains no EtOH chemistry. In combining the two schemes we have taken all of the elementary reactions of the MM-C_2H_2 set and appended 28 reactions from the LLNL-EtOH set to provide a pathway from EtOH to species that are treated in the MM-C_2H_2 set.

Since our CVD reactor temperatures are considerably higher than those encountered in typical combustion applications, there can be significant differences between the reaction paths that are important in the two cases. For example, the unimolecular dissociation reaction described below for CH_3CHO consumption is completely dominant only at very high temperatures. As another example, the H_2 dissociation reaction which is normally unimportant in combustion plays a crucial role under CVD reactor conditions. Throughout the paper it is important to keep in mind the differences between the CVD and combustion conditions and their effects on determining the dominant reaction paths.

The LLNL reaction scheme contains 23 reactions that directly involve EtOH. Although a rate-of-production analysis at a range of pressures from 0.001 to 1.0 atm and temperatures from 2500 K to 4000 K indicate that only 13 of the reactions make any detectable contribution to the EtOH chemistry, all 23 reactions were included in our reaction set. The only products of the EtOH chemistry that are not present in the Miller-Melius set are the species pC_2H_4OH, sC_2H_4OH, CH_3CHO, and C_2H_5O. The prefixes p and s on the C_2H_4OH species indicate that an H atom has been abstracted from the primary or secondary C, respectively. In order to merge the two reaction schemes, mechanisms have to be included which break down these products into species that are treated by the MM-C_2H_2 reaction set. Besides the reverse reactions which convert pC_2H_4OH back into EtOH, the only other reaction involving

this species is the unimolecular dissociation

$$pC_2H_4OH = C_2H_4 + OH. \tag{5}$$

Both reactions involving sC_2H_4OH lead to the formation of CH_3CHO,

$$sC_2H_4OH + M = CH_3CHO + H + M, \tag{6}$$

$$sC_2H_4OH + O_2 = CH_3CHO + HO_2. \tag{7}$$

The LLNL set contains a number of reactions involving CH_3CHO and C_2H_5O, but at the range of operating conditions considered, a rate-of-production analysis shows that the only reactions that make any detectable contribution to their consumption are the unimolecular dissociation reactions

$$CH_3CHO = CH_3 + HCO, \tag{8}$$

and

$$C_2H_5O = CH_3 + CH_2O. \tag{9}$$

Both of the reaction mechanisms used to construct our model were developed originally for combustion applications at temperatures significantly lower ($T \leq 2000$ K) than those encountered in typical CVD reactors ($T \geq 3000$ K). For the purpose of the present study, we have assumed that the temperature dependence of the reaction rates in these mechanisms can be extended to these higher temperatures. In most cases, higher temperatures simplify reaction mechanisms by reducing the number of reaction paths which are important, but details of the reaction mechanism, particularly those elements found to be most important, should be investigated at these higher temperatures in order to refine the model for future detailed studies.

B. Chemical kinetics approach

All of the chemical kinetics calculations were performed using the Sandia Chemkin program Perfectly Stirred Reactor (PSR) [16, 17]. The basic assumption of PSR is that the mixing of reactants is so complete that the conversion from reactants to products is totally dominated by the chemical reaction rates rather than diffusion, convection or other transport processes. The basic equations used in PSR are species conservation

$$\dot{m}(Y_k - Y_k^*) - \dot{\omega}_k W_k V = 0, \tag{10}$$

and energy conservation

$$\dot{m} \sum_{k=1}^{K} (Y_k h_k - Y_k^* h_k^*) + Q = 0, \tag{11}$$

where $\dot{m}$ is the mass flow rate through the reactor, V is the reactor volume, and Q is the reactor heat loss. The subscripted variables Y_k, W_k, and $\dot{\omega}_k$ are the mass fraction, molecular weight and production rate, respectively, of species k. The starred variables represent inlet conditions and the summation in the energy equation is over the number of species K. The mass flow rate through the reactor is related to the residence time τ in the reactor by the equation

$$\tau = \frac{\rho V}{\dot{m}}, \tag{12}$$

where ρ is the mass density in the reactor. The steady-state conservation equations are solved using a hybrid Newton/time-integration method. The PSR program can be used in one of two modes. Either the temperature and pressure of the reactor can be specified, in which case the K species conservation equations are solved, or the reactor heat loss and pressure are specified and the $K + 1$ species and energy equations are solved. In all of our simulations we assume that the reactor temperature and pressure are known and use PSR to calculate the species mole fractions in the reactor as a

function of time over the range from 1×10^{-3} s to 1×10^{3} s. Since by default PSR uses the results of a thermodynamic equilibrium calculation as the first guess for the outlet gas composition, it is easy to verify that the chemical kinetics calculations agree with thermodynamics in the limit of long residence times. For nearly all of our calculations the thermodynamic equilibrium conditions are closely approached for a residence time of 1000 s.

III. RESULTS

A. Divergence of species concentrations

One of the most striking features of the high-temperature $EtOH/H_2O$ chemistry is the sharp divergence in certain species concentrations as a function of inlet gas composition. For $[EtOH]/[H_2O]$ ratios below 1.0, corresponding to $[C]/[O] < 1$, the species O, OH, O_2, H_2O, and CO_2 are present in significant quantities (mole fractions $\geq 1 \times 10^{-5}$). As the inlet gas ratio is changed from below to above 1.0, the mole fractions of these oxygen-containing species drop dramatically while the mole fractions of the carbon-bearing species C, CH, CH_2, C_2, C_2H, and C_2H_2, and at higher pressures, CH_3 and CH_4, rise sharply. The mole fractions of the species CO, H, and H_2, in contrast, are relatively insensitive to the inlet gas composition and comprise the bulk of the outlet gases for the full range of conditions studied. The mole fractions of O, C, CO, H and H_2 are shown in Fig. 1 at T=3000 K and P=.001 atm. for inlet composition ratios $0.5 \leq [EtOH]/[H_2O] \leq 1.5$.

The key to understanding the divergence in species concentrations lies in the extreme stability of CO [19], which guarantees that as much CO as possible is formed from the available C and O. For an $EtOH/H_2O$ ratio exactly equal to one, the C/O ratio is also equal to one and virtually no C or O atoms remain free to form the other oxygen- or carbon-bearing species mentioned above. At inlet composition ratios

greater than one, nearly all of the O is tied up in the formation of CO, leaving an excess of C atoms to form the hydrocarbon and bare carbon species. Conversely, at inlet ratios below one, nearly all of the C is tied up forming CO, leaving an excess of O atoms to form the oxygen-bearing species.

The strong dependence of species concentrations on inlet gas composition observed in Figs. 1 are a generic property of the $EtOH/H_2O$ system and can be predicted solely on the basis of thermodynamics [18], but chemical kinetics calculations yield valuable information regarding the dependence of the details of the divergence on the operating conditions. To gain a deeper understanding of the divergence it is useful to look at the time dependence of the relative concentration $\xi_k(r_1, r_2, t)$, which we define as

$$\xi_k(r_1, r_2, t) = X_k(r_1, t)/X_k(r_2, t). \tag{13}$$

In this equation $X_k(r_1, t)$ and $X_k(r_2, t)$ are the mole fractions of species k at time t and inlet $EtOH/H_2O$ ratios r_1 and r_2, respectively. If values for r_1 and r_2 are chosen to be slightly above and slightly below one, respectively, then significant deviations of $\zeta_k(r_1, r_2, t)$ from one are indicative of the divergence. An advantage of studying ζ_k instead of X_k in this context is that it is easier to compare time scales and strengths of the divergences for different species regardless of their abundances.

Figures 2 show $\zeta_k(1.05, 0.95, t)$ for a temperature of 3000 K and a pressure range of 0.001-0.1 atm. for all of the major species except H, H_2 and CO. Several points regarding Figs. 2 are immediately obvious. First, the divergence in concentration for the different species all occur at roughly the same time. Second, groups of species can be identified which show nearly identical behavior. These groups are the C_2 group (C_2, C_2H, C_2H_2), the O_1 group (O, OH, H_2O, CO_2), and O_2. At high pressures the C_1 group (C, CH, CH_2, CH_3, CH_4) is clearly evident, but with decreasing pressure the

ζ_k for these species show significant variation. Third, the C_2 and O_2 species typically show a stronger divergence than the C_1 and O_1 species. We classify CO_2 as an O_1 species for the purpose of this study because CO, once formed, behaves essentially as an indivisible unit.

Because the divergence is a gradual process and shows some variations for different species, it is impossible to pinpoint an exact time at which the divergence occurs. Nonetheless, we find it useful to define an induction time, τ_1, which make it possible to identify trends in the divergence of species concentrations as a function of operating conditions. τ_1 is defined somewhat arbitrarily as the time at which the ζ_k either exceed 10.0 or drop below 10^{-1}. We find that τ_1 scales inversely with pressure, showing only small deviations at higher pressures, suggesting that the overall rate-controlling steps in our chemistry scheme are two-body rather than three-body reactions. τ_1 is shown in Fig. 3 as a function of pressure for several representative species.

In an effort to identify the overall rate-determining steps for the divergence, we have performed a sensitivity analysis of the dependence of induction time on the Arrhenius pre-exponential factors of the elementary reactions. At very short residence times, regardless of the inlet gas composition or reactor conditions, large amounts of CO, CH_3, CH_4, C_2H_2, H_2, and H_2O are present. The controlling factor in determining the induction time should be the rate of conversion of the inlet gases to the principal products CO, H, and H_2. Plots of the species mole fractions as a function of time show a correlation between the formation of H atoms and the divergence. This finding, together with the results of the sensitivity analysis shown in Table 1, suggests that the induction time is most sensitive to the reaction

$$H_2 + M = H + H + M. \tag{14}$$

The induction time is also found to depend, to a much lesser degree, on the rates of

the reactions $C_2H_2 + M = C_2H + H + M$ and $CO + H_2 = HCO + H$. Further analysis indicates that H atoms drive the divergence primarily through abstraction reactions. We have carried out calculations in which we first removed all reactions involving H atoms, with the exception of the dissociation/recombination reactions listed above and the H-atom abstraction reactions involving EtOH and its derivatives (pC_2H_4OH, sC_2H_4OH, CH_3CHO, and C_2H_5O), and then systematically replaced reactions until the divergence occurred. Restoring long-chain hydrocarbon reactions, $C_n, n \geq 3$, and reactions involving the breaking of C-C bonds, *i.e.*, $C_2H_2 + H = C + CH_3$, to the chemistry set has very little effect on the divergence. It is not until the hydrogen abstraction reactions involving C_1 and C_2 species are replaced that the divergence occurs on the timescales found using the full chemistry.

These results lead us to believe that the behavior of other alcohol/H_2O systems should be very similar to that of EtOH/H_2O. The rates for the initial steps in the dissociation of all alcohols, the removal of an H atom from either a primary or secondary carbon, should be very similar to the H atom abstraction rates for EtOH. The additional reactions required for the dissociation of higher alcohols, primarily the breaking of C-C bonds, would also be expected to be fast and not play a critical role in determination of induction times.

B. CO/CO_2 equilibrium

CO_2 deserves some special attention because it is the only species, with the exception of short-lived intermediate species and the predominating CO, which contains both carbon and oxygen and is present in significant quantities at high temperatures. The chemistry of CO_2 also is illustrative because it is typical of those species which are formed in significant quantities initially and then show a sharp increase or decrease in concentration at later times depending on the inlet gas composition. In

the remainder of this section we describe the relevant reactions which establish the CO/CO_2 equilibrium.

Various oxygen-bearing species can attack CO to form CO_2, but a rate-of-production analysis shows that CO_2 is formed almost exclusively by the reaction

$$CO + OH = CO_2 + H. \tag{15}$$

The CO_2 either reacts to directly form CO or forms the species HCO or CH_2O which in turn react to form CO via the reactions,

$$CO_2 + CH = HCO + CO, \tag{16}$$

$$CO_2 + CH_2 = CH_2O + CO, \tag{17}$$

$$CO_2 + H = HCO + O, \tag{18}$$

$$CO_2 + M = CO + O + M, \tag{19}$$

$$CO_2 + CH_2^* = CH_2O + CO. \tag{20}$$

In the last reaction listed above, CH_2^* is the excited singlet state of CH_2. The species CH_2O is converted to HCO, primarily by interacting with H but also by interacting with OH and third bodies, through the reactions

$$CH_2O + H = HCO + H_2, \tag{21}$$

$$CH_2O + OH = HCO + H_2O, \tag{22}$$

$$CH_2O + M = HCO + H + M. \tag{23}$$

HCO then forms CO through

$$HCO + M = CO + H + M, \tag{24}$$

$$HCO + OH = CO + H_2O, \tag{25}$$

$$HCO + H = CO + H_2. \tag{26}$$

Through the above sets of reactions, an equilibrium will be established between CO and CO_2. It is important to note that the only reaction pathways which exist for the conversion of CO into CO_2 involve the oxygen containing species O, O_2, OH and HO_2, while the conversion of CO_2 back to CO can occur via reactions involving CH, CH_2, H, and third bodies. For this reason, after long residence times negligible amounts of CO_2 are found for inlet composition ratios above one, since all of the CO_2 that is formed is rapidly converted to CO.

C. H/H_2 equilibrium

Hydrogen plays a critical role in the growth of diamond films [19]. Previous studies have shown that both the quality and the growth rates of the diamond films depend critically on the H atom concentration [19, 20]. Although there are a number of theories promoting various growth mechanisms, it is almost universally accepted that a crucial stage in the growth process involves the abstraction of a hydrogen atom from the diamond surface through the reaction

$$CH(S) + H = C(S,R) + H_2, \tag{27}$$

where CH(S) is a hydrogen terminated surface carbon and C(S,R) is a surface radical [21]. The surface site created in this way can now accept one of the carbon growth species. In addition to initiating surface growth, H atoms also plays the key role in terminating the surface through the reaction

$$C(S,R) + H = CH(S). \tag{28}$$

An analysis of the conditions which lead to the growth of high-quality diamond indicate that a minimum of $10^{4.24\pm0.21}$ ($\sim$ 10000-30000) H atoms must strike the diamond surface for every carbon atom that is incorporated on the surface [22]. Although this paper is focusing primarily on gas phase chemistry, it is appropriate to consider

surface chemistry from the point of view that these calculations could represent the infinite limit boundary conditions on a 1D transport or a 3D reactive flow calculation. With this emphasis in mind, it is now appropriate to consider what range of residence times and inlet gas compositions give rise to optimal H/CH_x boundary conditions. Neglecting boundary layer effects and assuming that all CH_x species have the same sticking probability after encountering an open surface site, we can make the following estimate of the ratio of H atoms striking the surface to carbon atoms incorporated,

$$\Psi = \frac{X_H/\sqrt{m_H}}{(\sum_{x=0}^{4} X_{CH_x}/\sqrt{m_{CH_x}})\gamma Z}, \tag{29}$$

where γ is the sticking probability and Z is the fraction of surface sites that are open. We used the values of $\gamma = 0.33$ and $Z = 0.05$ taken from the work of Coltrin and Dandy [23]. Ψ is displayed in Fig. 4 for a range of inlet gas compositions at P=0.001 atm. and T=3000 K. At short residence times, before the sharp divergence in species concentrations as a function of inlet gas composition occurs, the ratio of H atoms impacting the surface to carbon atoms incorporated is much too small for high-quality diamond growth. Using an $EtOH/H_2O$ ratio of 1.5 yields values of Ψ that are slightly below the critical value for diamond growth, while an $EtOH/H_2O$ ratio equal to 1.1 results in values of Ψ consistent with diamond growth. Although Fig. 4 shows that for water-rich inlet gas compositions the values of Ψ are well above the critical value, it is unlikely that diamond growth can occur under these conditions because of the large concentrations of species such as O, O_2, and OH which have a tendency to etch the surface [24].

We have carried out calculations on both pure hydrogen and $EtOH/H_2O$ mixtures to determine the H/H_2 equilibrium. The equilibrium constant in the pure hydrogen system is defined as $K_{eq} \equiv [H]/[H_2]$. For the $EtOH/H_2O$ mixtures we also define an effective equilibrium constant K'_{eq} which is the $[H]/[H_2]$ ratio that is established

when the entire reaction set is considered. Over a large range of pressures, temperatures, and inlet compositions the effective equilibrium constant lies within the range $1.21K_{eq} \leq K'_{eq} \leq 1.31K_{eq}$. Thus the presence of the other species in the $EtOH/H_2O$ system shifts the H/H_2 equilibrium slightly in the direction of atomic hydrogen. Although the change in the H/H_2 equilibrium is small, it is advantageous that the shift is towards higher H concentrations because of the critical role of H atoms in diamond growth. The relative insensitivity of K'_{eq} to inlet composition suggests that the species CO, which is itself insensitive to inlet composition, is principally responsible for the shift in H/H_2 equilibrium. Rate-of-production analysis shows that CO drives the equilibrium in the direction of excess H through the reaction sequence

$$CO + H_2 = HCO + H \tag{30}$$

$$HCO + M = H + CO + M. \tag{31}$$

The equilibrium H/H_2 ratios for pure H/H_2 and $EtOH/H_2O$ are shown in Fig. 5. These curves suggest a range of possible operating conditions for a diamond CVD reactor. For example, even at very low pressures it is unlikely that sufficient H atoms will be produced at reactor temperatures below 2500 K for thermal plasmas that are neutral dominated. It should be noted that the equilibrium results shown in Fig. 5 constitute upper limits on the H/H_2 ratio. At short residence times, the H/H_2 ratio for the $EtOH/H_2O$ mixture is very small. Since H atom production follows primarily from the dissociation of H_2, the equilibrium ratios are approached from below in the limit of long residence time. In addition, these ratios are very temperature-sensitive. Since in a diamond CVD reactor the substrate temperatures are typically around 1000 K, significant recombination of H atoms can occur as the atoms diffuse from the hot interior of the reactor toward the cooler surface.

D. Relative concentrations of C_1 and C_2 species

Although a gradual transition from diamond growth to graphitic growth occurs as the C/H ratio increases [4], there is uncertainty over which C species are responsible for each type of growth. Some studies suggest that the C_1 species are necessary for diamond growth while C_2 species lead to the formation of graphite. Coltrin and Dandy [23] support this view by arguing on the basis of thermodynamics that the surface adsorption of C_2H_2 is energetically unfavorable as a precursor to diamond but energetically favorable for graphitic growth. Frenklach, on the other hand, has proposed a plausible surface reaction scheme for the growth of diamond from C_2H_2 [25, 26]. Rather than investigating the validity of these and other proposals, we shall confine ourselves to simply making predictions about the relative abundances of the C_1 and C_2 species as a function of reactor inlet gas composition, temperature, pressure, and residence time.

The results of simulations at temperatures ranging from pressures ranging from 0.001-0.1 atm. show that the dominant C species at higher pressures and lower temperatures is C_2H_2. As the reactor temperature is increased and the pressure is decreased, atomic C becomes the most abundant species. A crossover from C_2H_2 to C dominance is observed at a residence time of approximately 10 s for a temperature of 3000 K and pressures of 0.001-0.01 atm. All of these results are illustrated in Figs. 6, 7, and 8. In addition to the temperature and pressure dependencies, the inlet gas composition is also seen to have an affect on the ratio of C_1 to C_2 species. Figure 9 shows that the ratios $[C]/[C_2]$, $[C]/[C_2H]$, and $[C]/[C_2H_2]$ all increase as the $[EtOH]/[H_2O]$ ratio approaches one from above.

IV. SUMMARY

In our study of the high-temperature chemistry of EtOH-H_2O we have made

a number of observations that may have an impact on the use of these feedstocks for diamond CVD reactors. The main finding of this work is the existence of the sharp divergence in the species mole fractions as the inlet $EtOH/H_2O$ ratio is tuned from below to above one. Our analysis indicates that the divergence is due to the stability of CO and that the primary rate-limiting step determining the characteristic induction time is the dissociation reaction $H_2 + M = H + H + M$. At short residence times, before the divergence occurs, other oxygen- and carbon-bearing species are present in significant quantities.

Although our simulations do not explicitly include surface chemistry, we can still make rough predictions of the operating conditions that will lead to diamond growth. Because of the relatively low H atom mole fraction before the divergence, and the prominent role of atomic hydrogen in promoting diamond growth in CVD reactors [19], it is likely that optimal diamond growth will only occur at longer residence times. In this limit the picture is completely different. For $EtOH/H_2O$ ratios less than one, the mole fractions of the potential growth species drop dramatically after the divergence occurs, making it unlikely that diamond growth will occur. Indeed, the availability of O, OH, and O_2 to attack the diamond surface suggests that any diamond film will be etched [24]. For $EtOH/H_2O$ ratios greater than one, on the other hand, the growth-species concentrations remain high after the divergence takes place and nearly all of the oxygen is tied up in CO. The abundance of H atoms after this split suggests a favorable environment for diamond film growth.

Although we have made no predictions concerning the roles of different species in diamond or non-diamond carbon growth, we are able to predict the mole fractions of the various species as a function of operating conditions such as the reactor residence time, temperature, pressure and inlet gas composition. One of the main findings is a crossover from C_2H_2 to C as the predominant non-CO carbon species as the

reactor temperature is increased and the pressure is decreased. Another important result is that the ratios of C_1 to C_2 species increase as the $EtOH/H_2O$ inlet ratio approaches one from above. If models based on diamond growth from C_1 species and non-diamond carbon growth from C_2 species are correct, then this result would be consistent with a transition from diamond to non-diamond growth as the relative EtOH concentration is increased.

ACKNOWLEDGMENTS

The authors thank our NRL colleagues K. Kailasanath, Elaine S. Oran, Jay P. Boris, and James E. Butler for useful suggestions regarding this work and Gopal Patnaik for getting us started with Chemkin. We appreciate help from Raymond E. Thomas and Ronald A. Rudder of Research Triangle Institute and David G. Goodwin of California Institute of Technology for educating us on many of the practical aspects of diamond CVD. Prof. Goodwin also kindly provided us with the Miller-Melius reaction set in Chemkin format. RSS thanks David Hodo. This research was supported by the thermal management program of the Advanced Research Projects Agency.

REFERENCES

[1] F.G. Celli and J.E. Butler, Ann. Rev. Chem. **42**, 643 (1991).

[2] W. Eversole, U.S. Patents 3030187, 3030188, 1962 (filed 1959).

[3] H.J. Hibsman, U.S. Patent 3371996, 1968 (filed 1964).

[4] P.K. Bachmann, D. Leers, and H. Lydtin, Diamond Relat. Mater. **1**, 1 (1991).

[5] M. Buck, T.J. Chuang, J.H. Kaufman, and H. Seki, Mater. Res. Soc. Symp. Proc. **162**, 97 (1990).

[6] L. Kostadinov and D. Dobrev, Surf. Coat. Technol. **47**, 623 (1991).

[7] R.A. Rudder, G.C. Hudson, J.B. Posthill, R.E. Thomas, R.C. Hendry, D.P. Malta, R.J. Markunas, T.P. Humphreys, and R.J. Nemanich, J. Appl. Phys. **60**, 329 (1991)

[8] E.Y. Garcia and M.A. Laborde, Int. J. Hydrogen Energy **16**, 307 (1991).

[9] S.J. Harris and A.M. Weiner, Appl. Phys. Lett. **55**, 2179 (1989).

[10] J.A. Mucha, D.L. Flamm, and D.E. Ibbotson, J. Appl. Phys. **65**, 3448 (1989).

[11] I. Schmidt, C. Benndorf, and P. Joeris, Proc. of 8th CiMTEC - World Ceramic Congress and Forum on New Materials, 1994 [in press].

[12] E. Meeks, R.J. Kee, D.S. Dandy, and M.E. Coltrin, Comb. Flame **92**, 144 (1993).

[13] Y. Matsui and M. Sahara, Jpn. J. Appl. Phys. **28**, 1023 (1989).

[14] J.A. Miller and C.F. Melius, Comb. Flame **91**, 21 (1992).

[15] H.J. Curran, M.P. Dunphy, J.M. Simmie, C.K. Westbrook, and W.J. Pitz, 24th Symposium (Int'l) on Combustion, Combustion Institute, 769 (1992).

[16] P. Glarborg, R.J. Kee, J.F. Grcar, and J.A. Miller, Sandia National Laboratories Report, SAND89-8209 (1993).

[17] R.J. Kee, F.M. Rupley, and J.A. Miller, Sandia National Laboratories Report, SAND89-8009B (1994).

[18] N.A. Prijaya, J.C. Angus, and P.K. Bachmann, Diamond Relat. Mater. **3**, 129 (1993).

[19] J.E. Butler and R.L. Woodin, Phil. Trans. R. Soc. Lond. A **342**, 209 (1993).

[20] D.G. Goodwin, J. Appl. Phys. **74**, 6888 (1993).

[21] B.D. Thoms, J.N. Russell, Jr., P.E. Pehrson, and J.E. Butler, J. Chem. Phys. **100**, 8425 (1994).

[22] D.G. Goodwin, private communication.

[23] M.E. Coltrin and D.S. Dandy, J. Appl. Phys. (submitted).

[24] R.E. Thomas, R.A. Rudder, and R.J. Markunas, J. Vac. Sci. Tech. A **10**, 2451 (1992).

[25] M. Frenklach, J. Appl. Phys. **65**, 5142 (1989).

[26] M. Frenklach and H. Wang, Phys. Rev. **B43**, 1520 (1991).

TABLES:

TABLE 1. Induction times τ_1 for the species C and O under operating conditions T=3000 K and P=.01 atm. The induction times listed in the first table entry were obtained using the original unmodified chemistry. The subsequent induction times were obtained for the Arrhenius pre-exponential factor of the corresponding reaction multiplied by ten. The effects of modifying all other reaction pre-exponential factors are small and are not shown.

chemistry	τ_1(C)	τ_1(O)
unmodified	0.41	0.28
$H + H + M = H_2 + M$	0.17	0.13
$H + H + H_2 = H_2 + M$	0.16	0.11
$C_2H_2 + M = C_2H + H + M$	0.33	0.29
$HCO + H = CO + H_2$	0.38	0.25

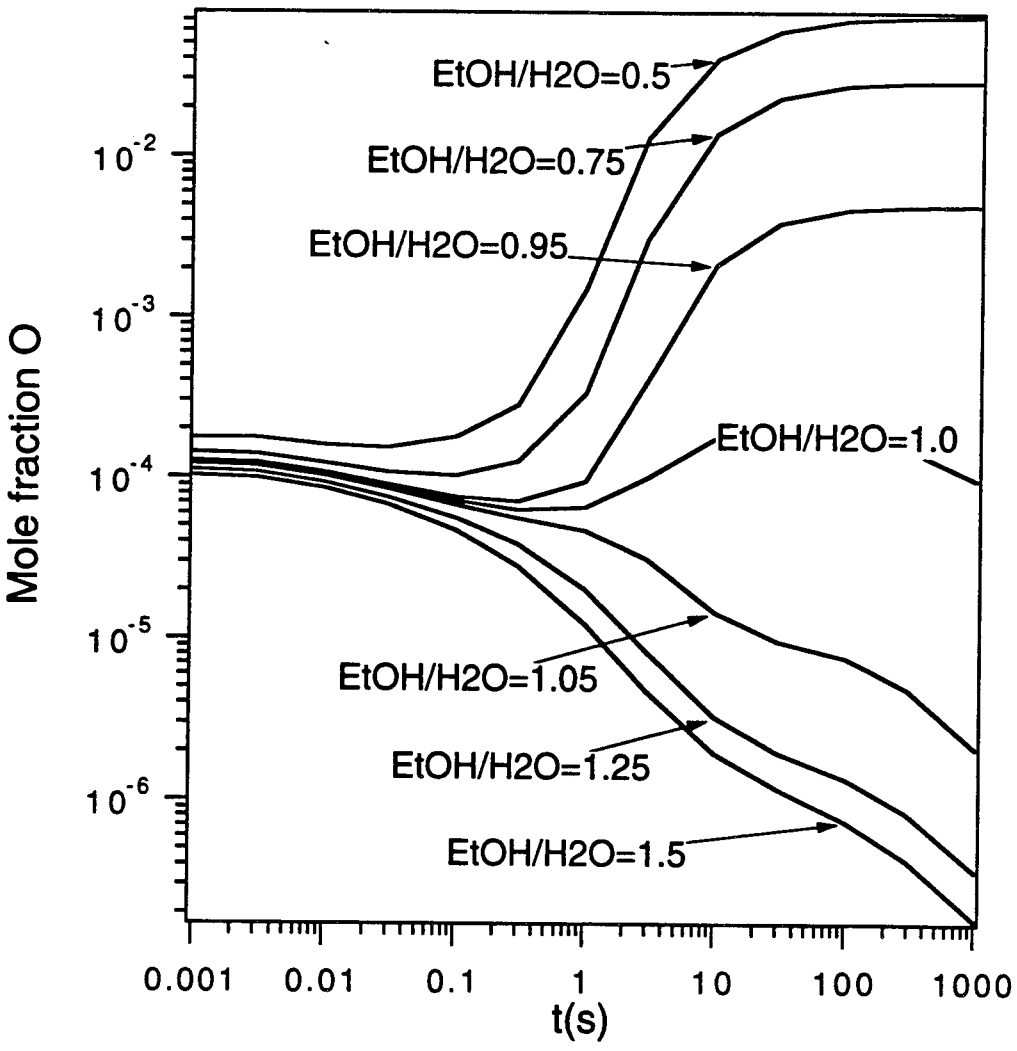

(a)

Fig. 1 — Time-dependent mole fractions of the species (a) O, (b) C, (c) CO, (d) H, and (e) H_2 for T=3000 K and P = .001 atm. for a range of inlet [EtOH]/[H_2O] ratios ranging from 0.5 to 1.5.

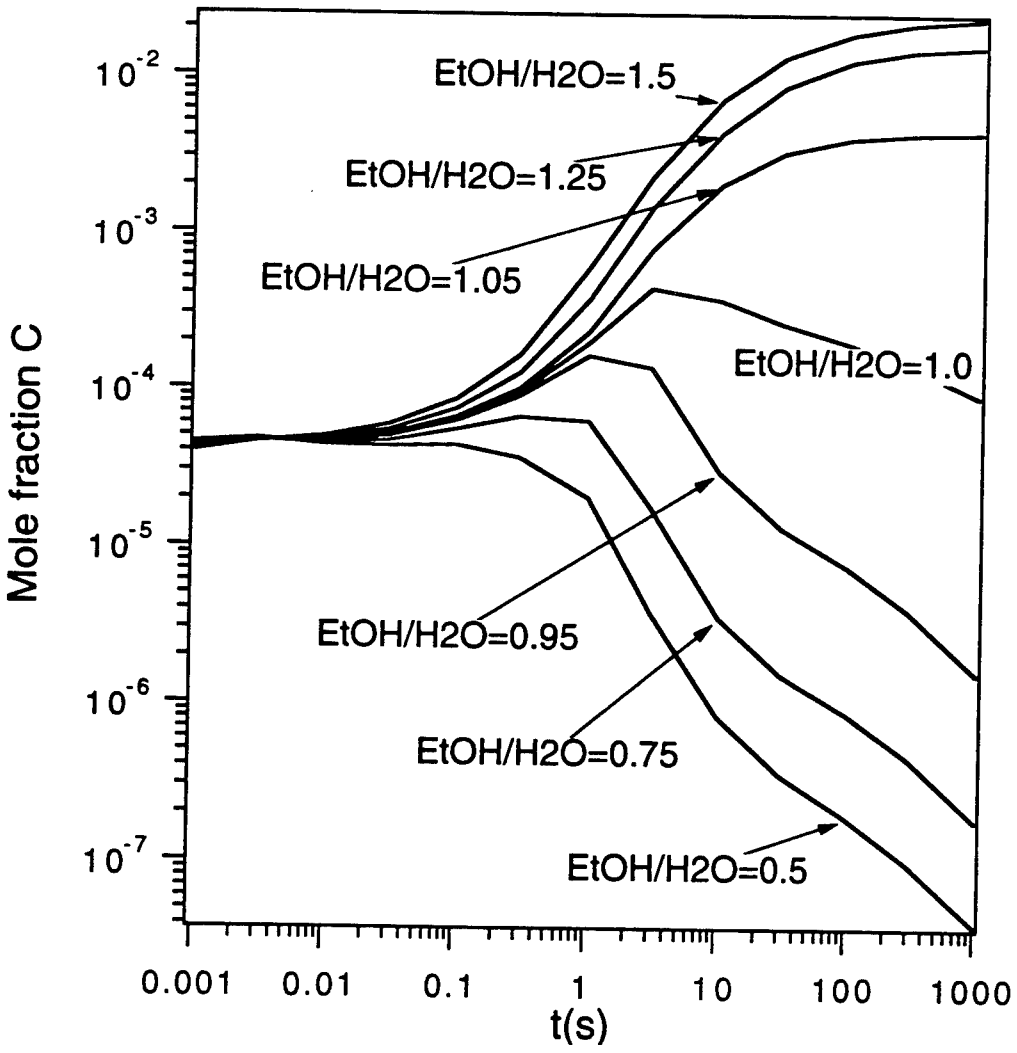

(b)

Fig. 1 — (Continues) Time-dependent mole fractions of the species (a) O, (b) C, (c) CO, (d) H, and (e) H_2 for T=3000 K and P = .001 atm. for a range of inlet [EtOH]/[H_2O] ratios ranging from 0.5 to 1.5.

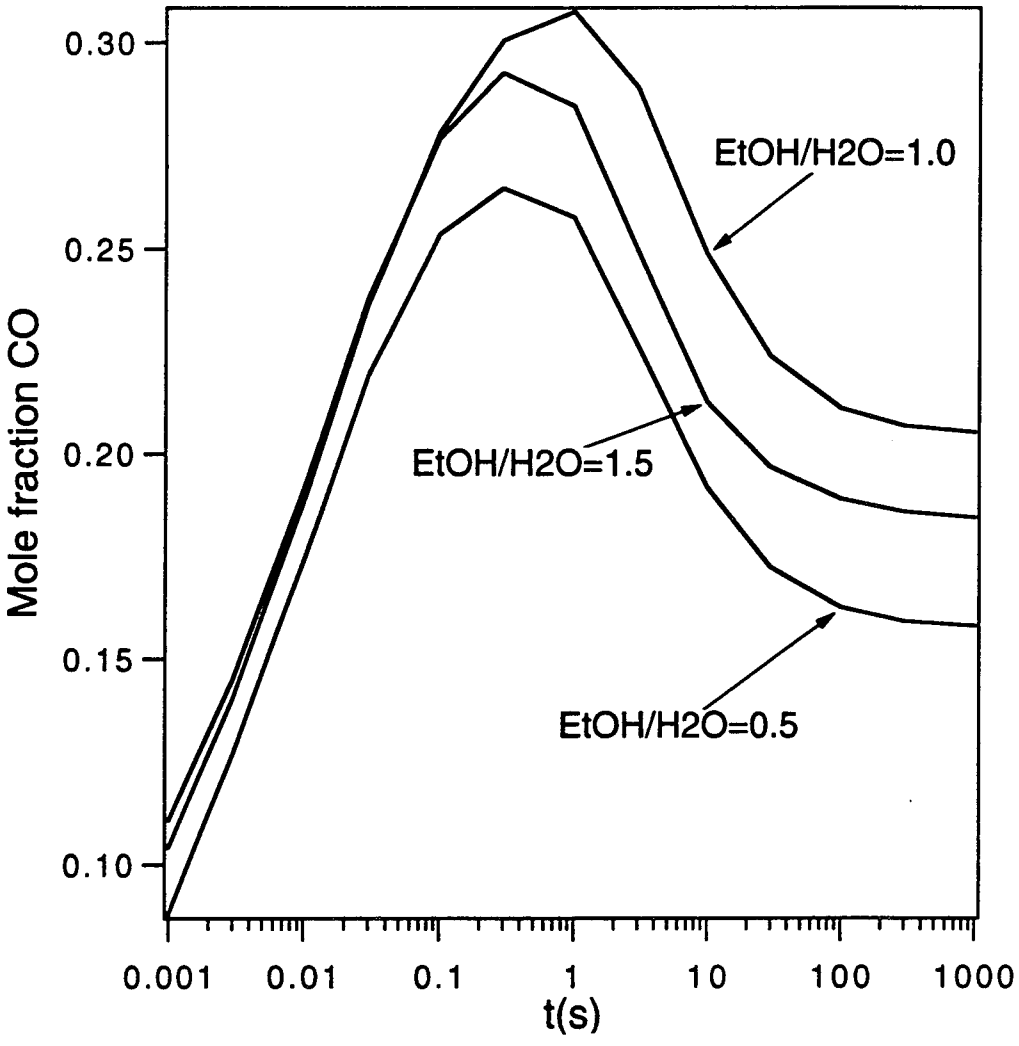

(c)

Fig. 1 — (Continues) Time-dependent mole fractions of the species (a) O, (b) C, (c) CO, (d) H, and (e) H_2 for T=3000 K and P = .001 atm. for a range of inlet [EtOH]/[H_2O] ratios ranging from 0.5 to 1.5.

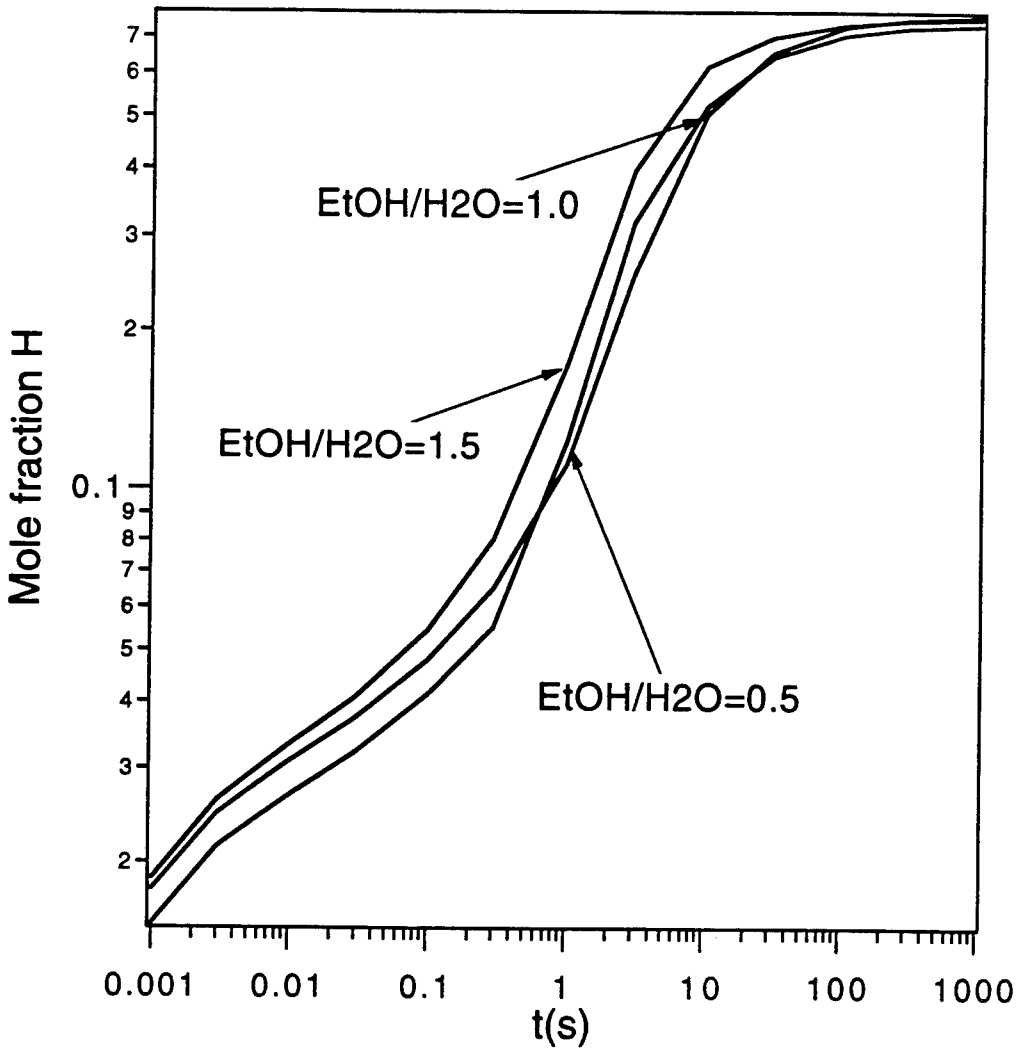

(d)

Fig. 1 — (Continues) Time-dependent mole fractions of the species (a) O, (b) C, (c) CO, (d) H, and (e) H_2 for T=3000 K and P = .001 atm. for a range of inlet [EtOH]/[H_2O] ratios ranging from 0.5 to 1.5.

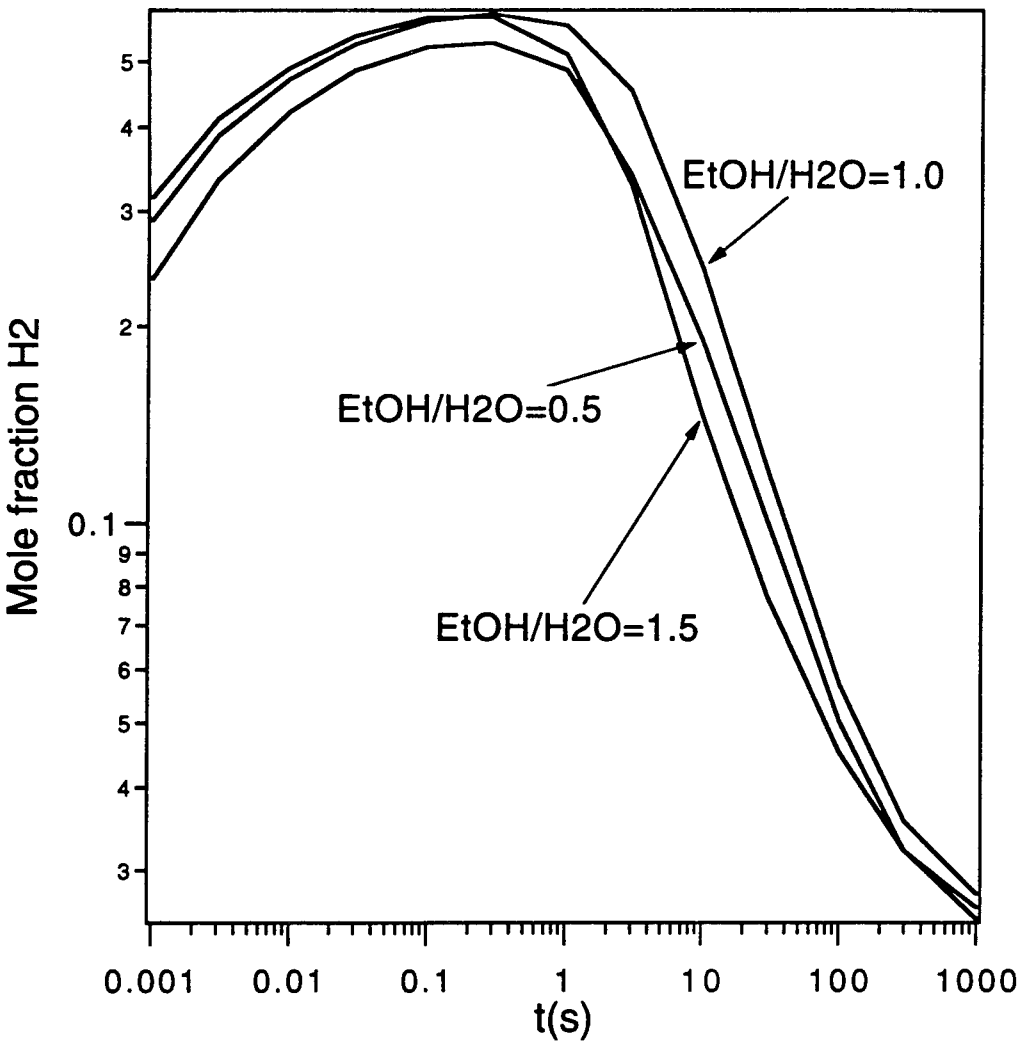

(e)

Fig. 1 — (Continues) Time-dependent mole fractions of the species (a) O, (b) C, (c) CO, (d) H, and (e) H_2 for T=3000 K and P = .001 atm. for a range of inlet [EtOH]/[H_2O] ratios ranging from 0.5 to 1.5.

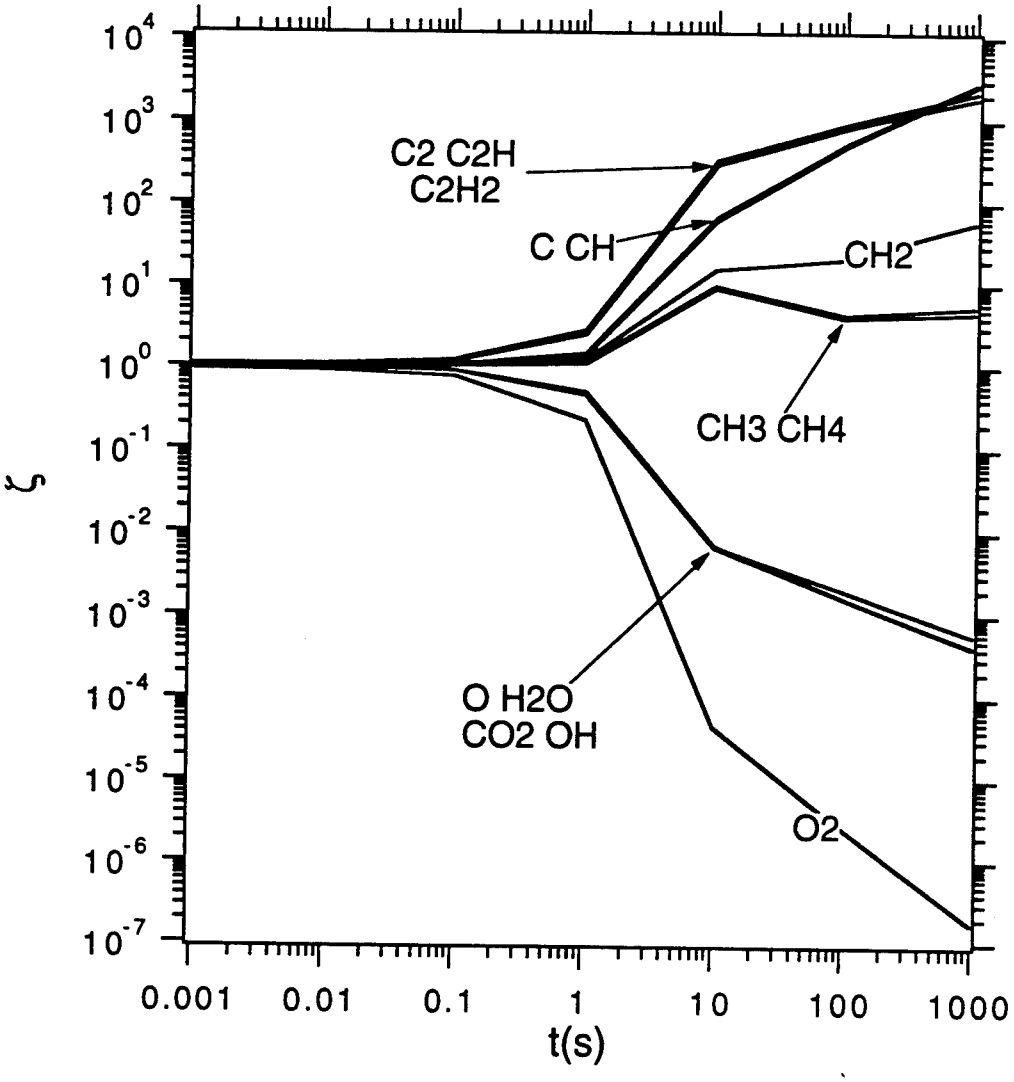

(a)

Fig. 2 — Relative concentrations ζ_k vs. time for $r_1 = 1.05$, $r_2 = 0.95$ and a reactor temperature of 3000 K for pressure equal to (a) 0.001 atm., (b) 0.01 atm., and (c) 0.1 atm. ζ_k is defined in Eq. 13 in section IIIa.

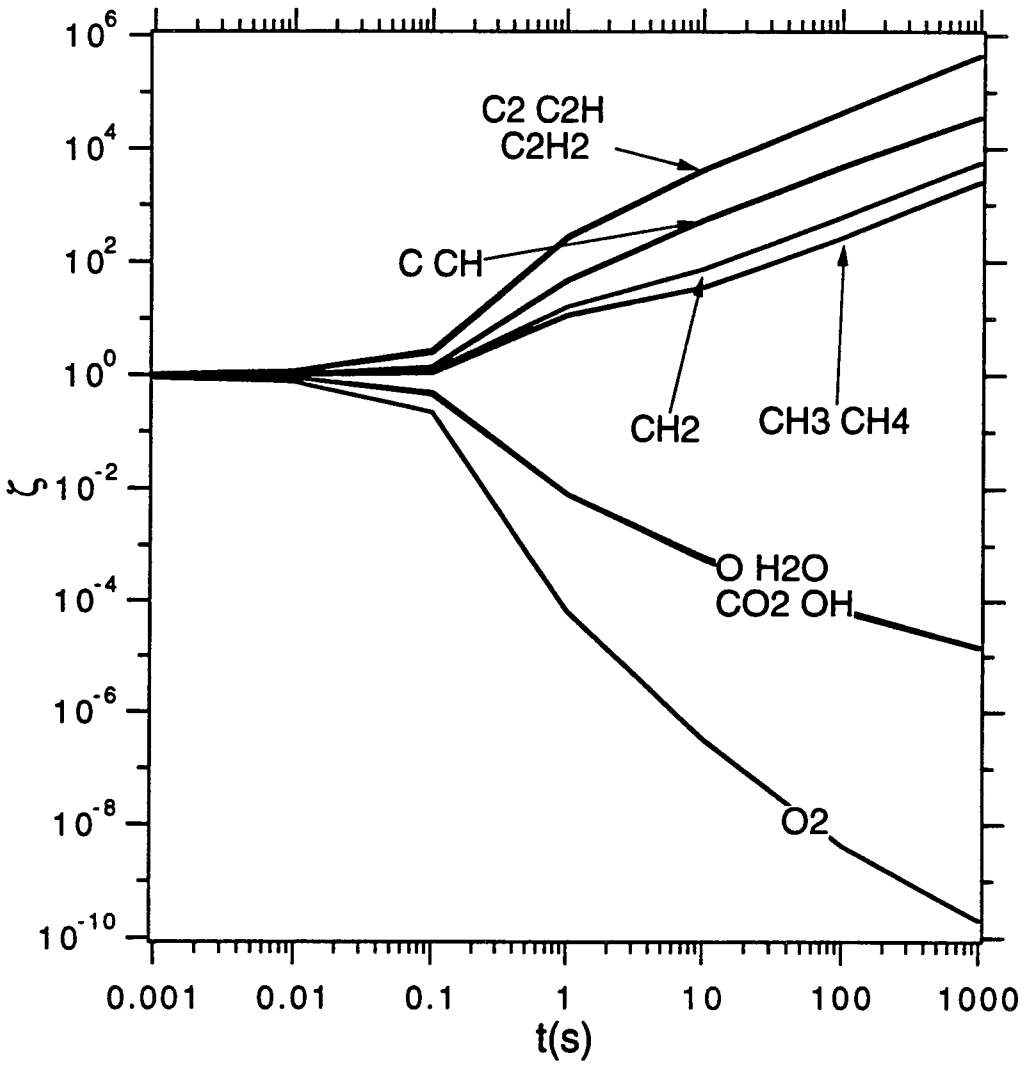

(b)

Fig. 2 — (Continues) Relative concentrations ζ_i vs. time for $r_1 = 1.05$, $r_2 = 0.95$ and a reactor temperature of 3000 K for pressure equal to (a) 0.001 atm., (b) 0.01 atm., and (c) 0.1 atm. ζ_i is defined in Eq. 13 in section IIIa.

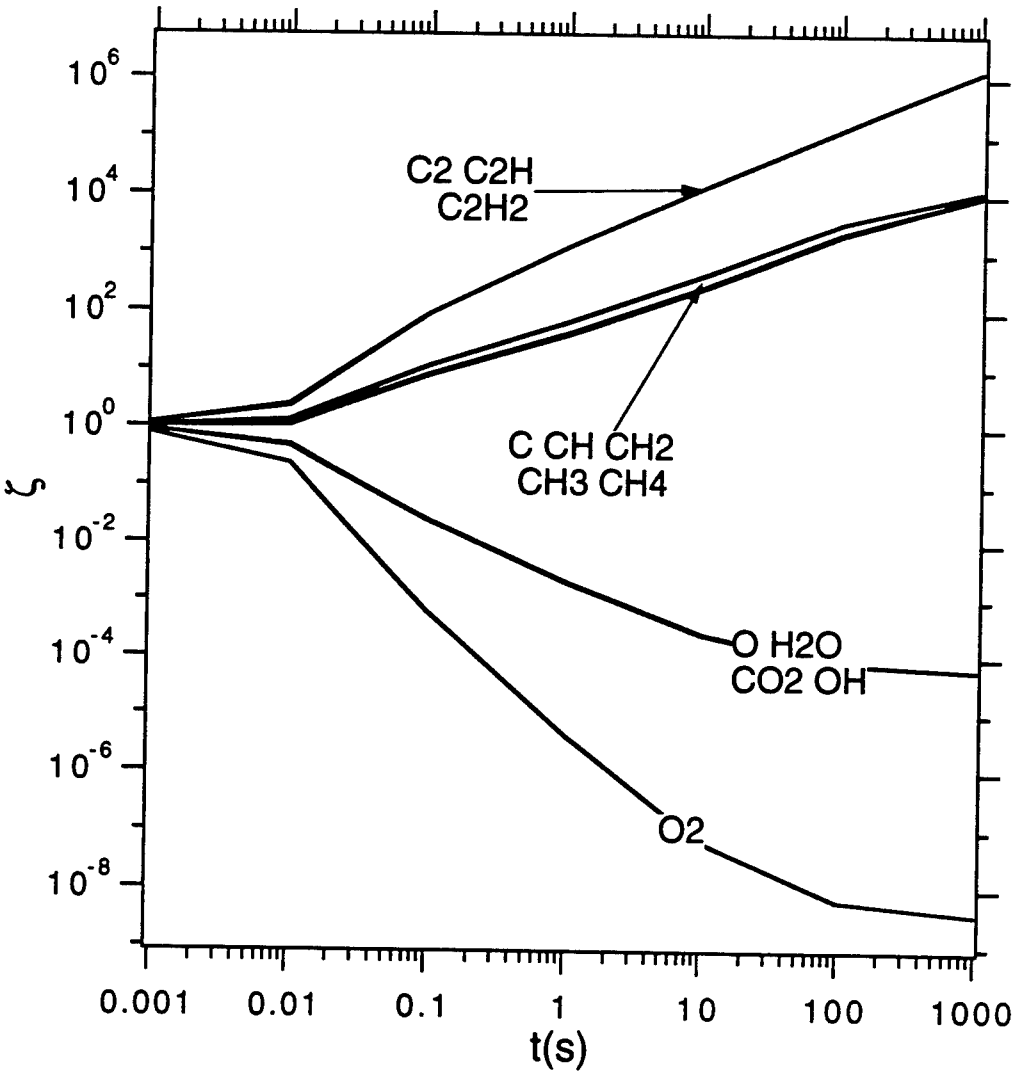

(c)

Fig. 2 — (Continues) Relative concentrations ζ_i vs. time for $r_1 = 1.05$, $r_2 = 0.95$ and a reactor temperature of 3000 K for pressure equal to (a) 0.001 atm., (b) 0.01 atm., and (c) 0.1 atm. ζ_i is defined in Eq. 13 in section IIIa.

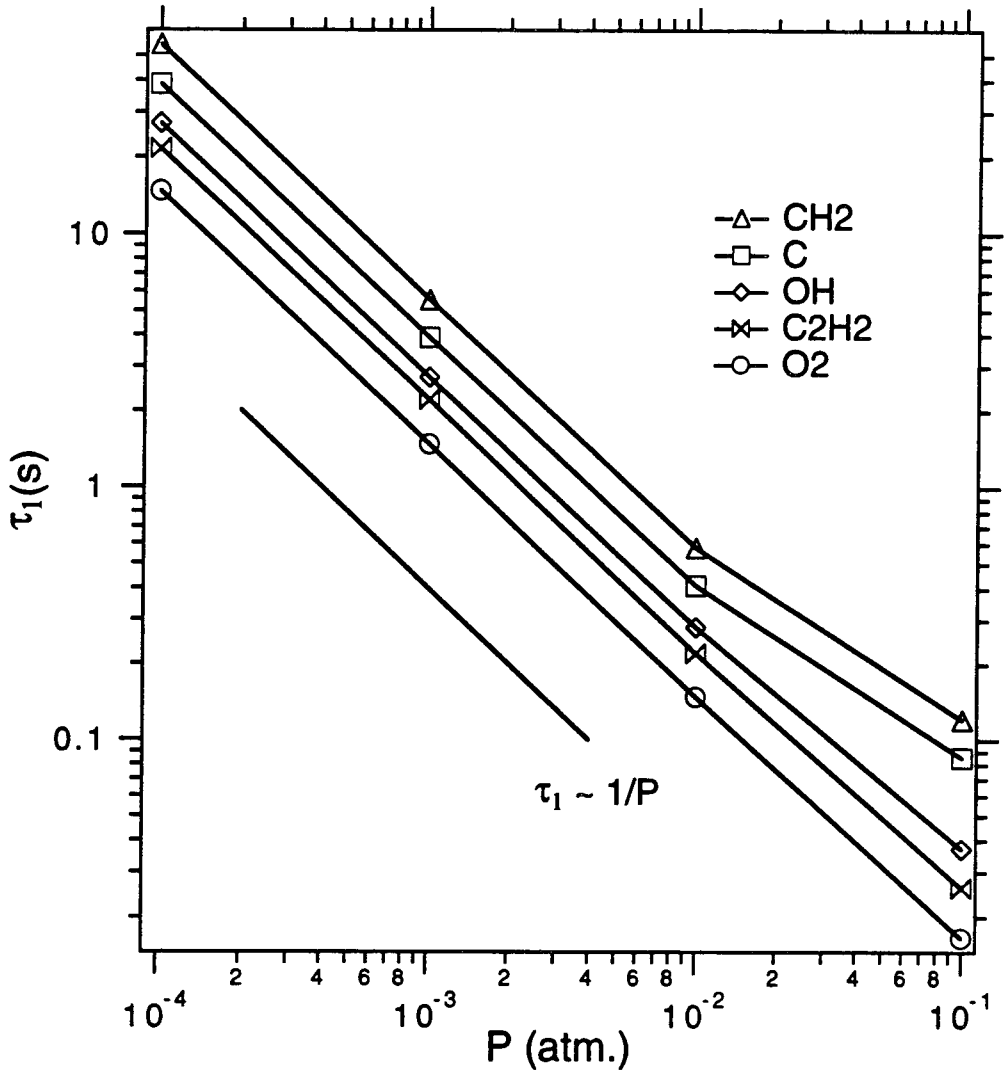

Fig. 3 — Induction times τ_1 as a function of pressure at T=3000 K for several representative species. τ_1 is defined as the time at which ζ_k either exceeds 10.0 or drops below 0.01 for inlet composition ratios of $r_1 = 1.05$ and $r_2 = 0.95$.

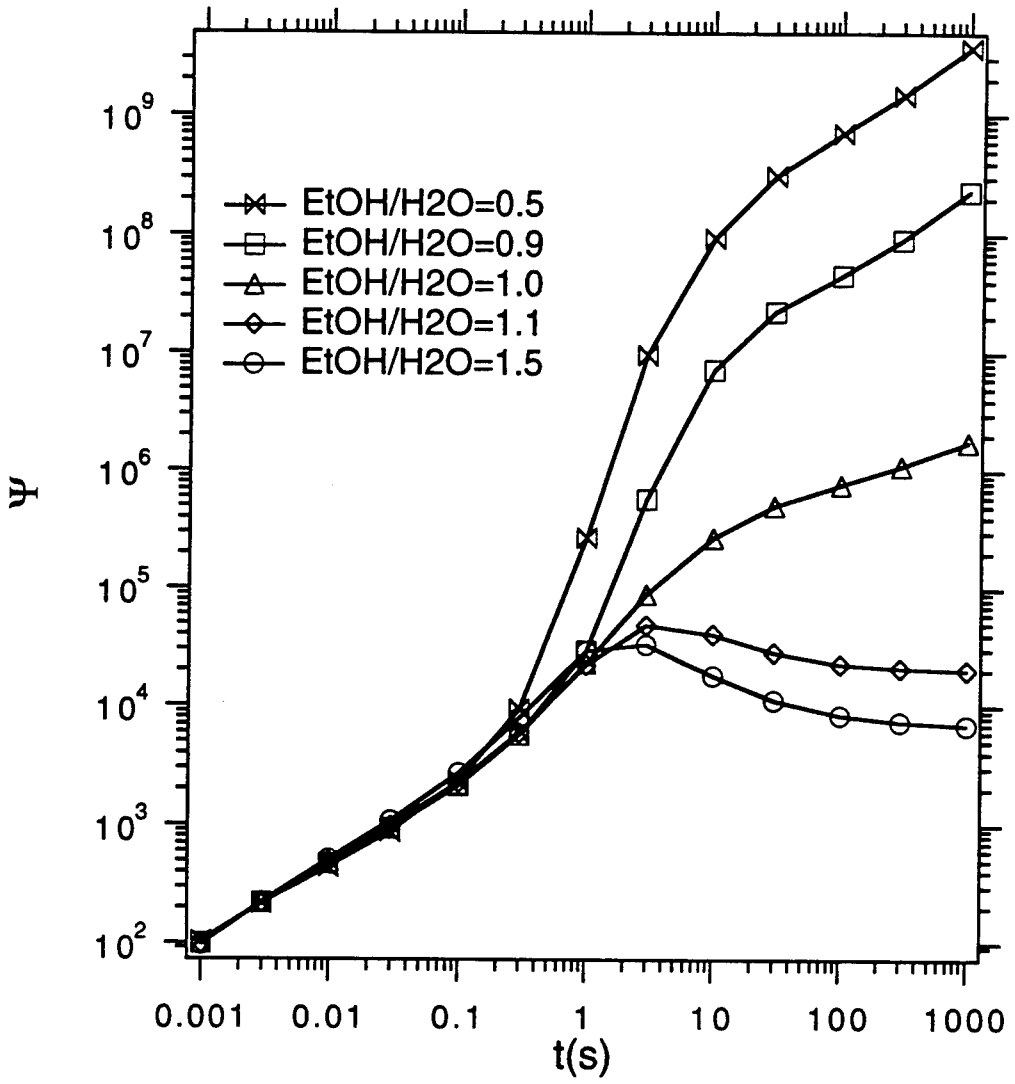

Fig. 4 — Estimated ratio Ψ of H atoms impacting the surface to carbon atoms incorporated on the surface as a function of residence time for operating conditions P=0.001 atm. and T=3000K.

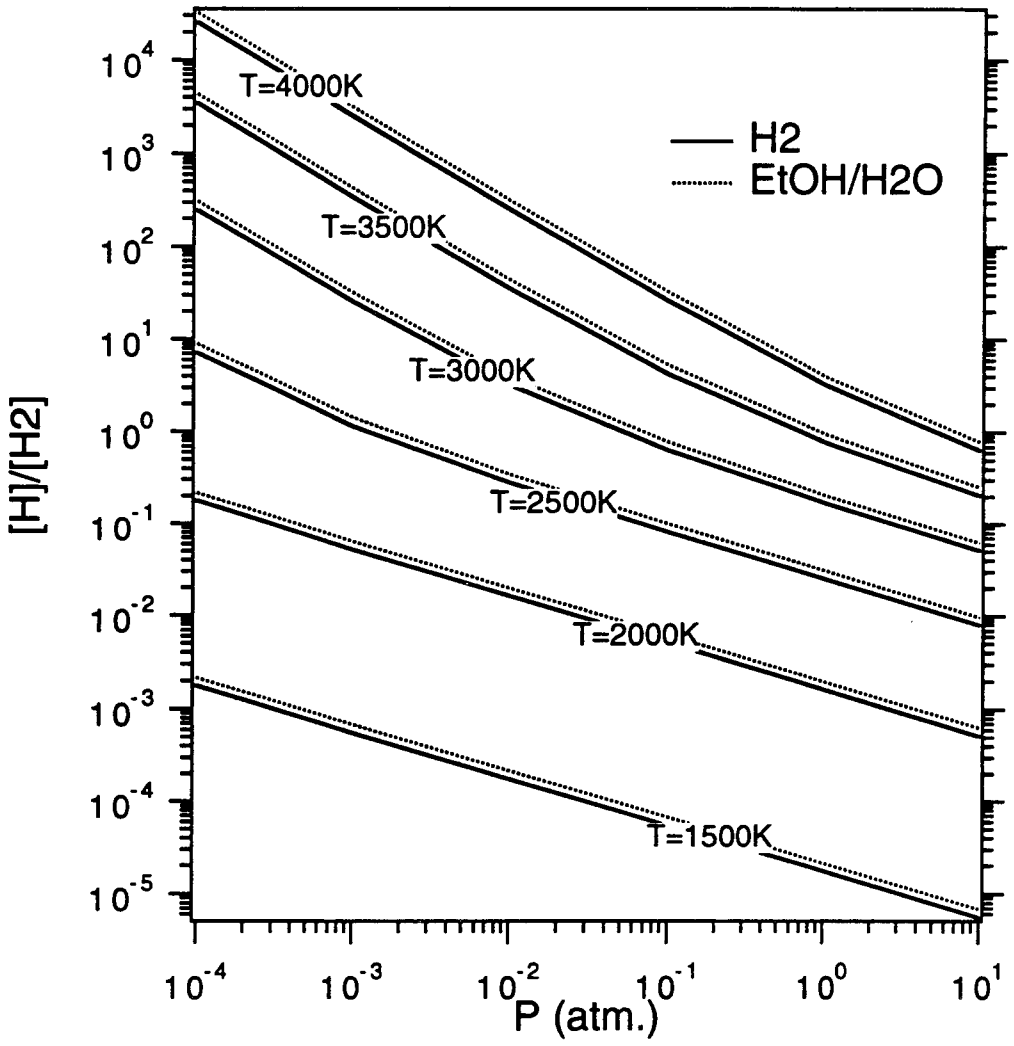

Fig. 5 — $[H]/[H_2]$ equilibrium ratios in pure hydrogen (solid lines) and $EtOH/H_2O$ (dashed lines).

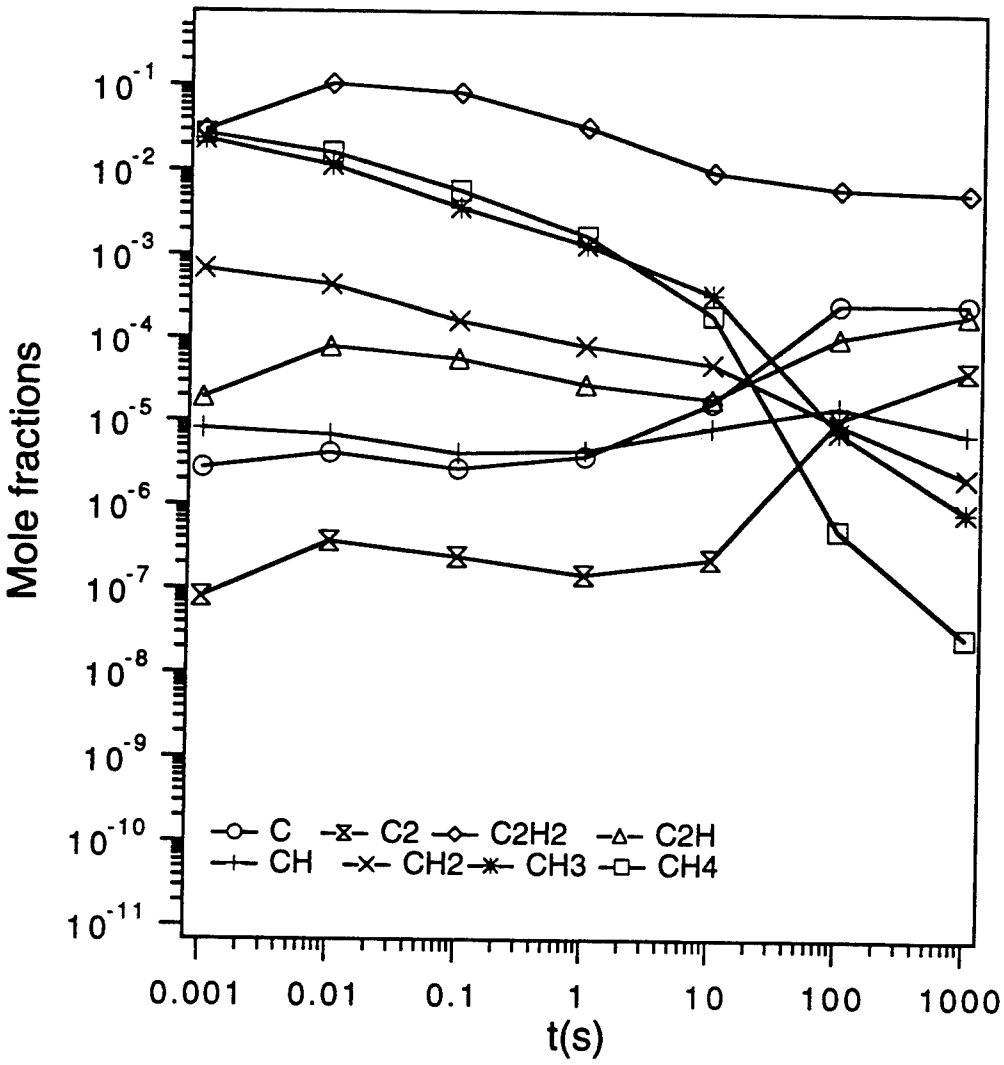

(a)

Fig. 6 — Mole fractions of carbon-containing species at T=2500 K and inlet [EtOH]/[H_2O] ratio 1.1 at pressure equal to (a) 0.001 atm., (b) 0.01 atm., and (c) 0.1 atm.

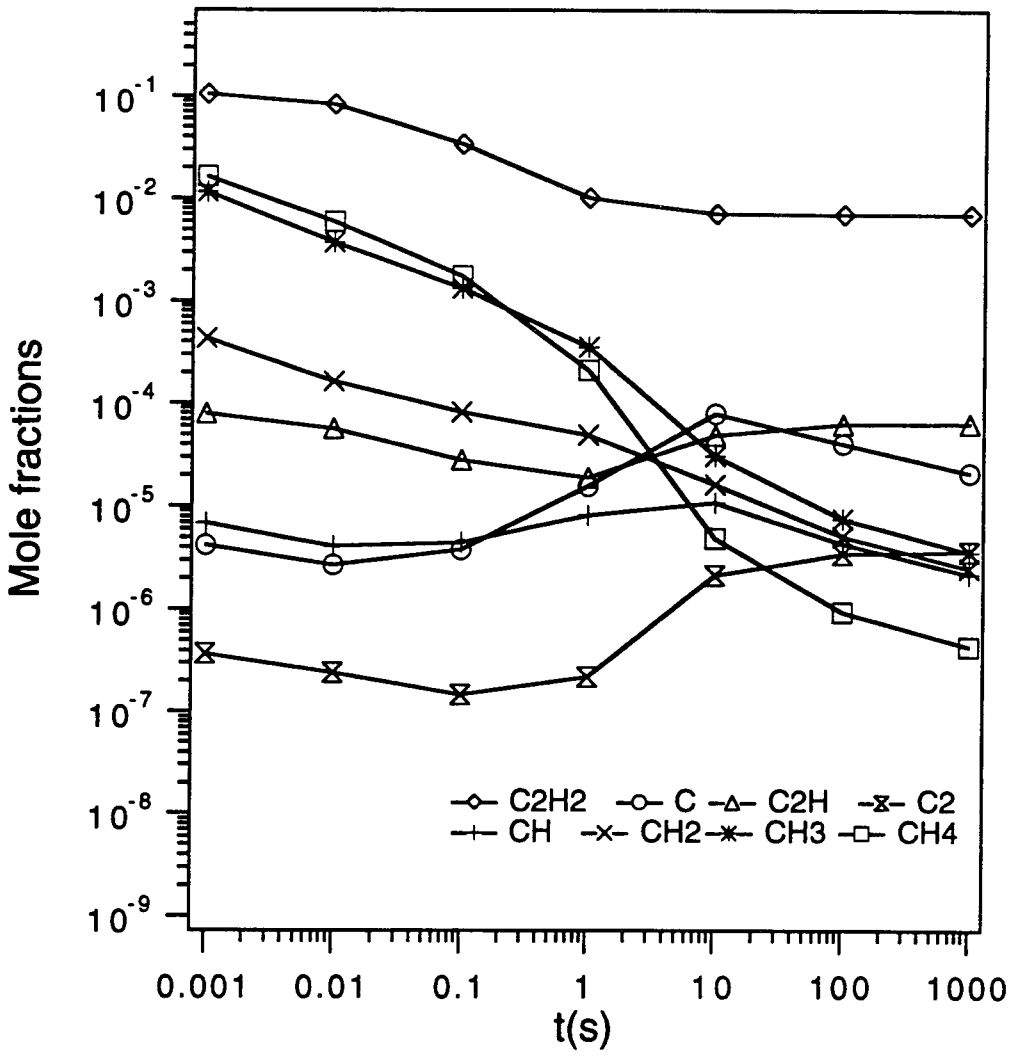

(b)

Fig. 6 — (Continues) Mole fractions of carbon-containing species at T=2500 K and inlet [EtOH]/[H_2O] ratio 1.1 at pressure equal to (a) 0.001 atm., (b) 0.01 atm., and (c) 0.1 atm.

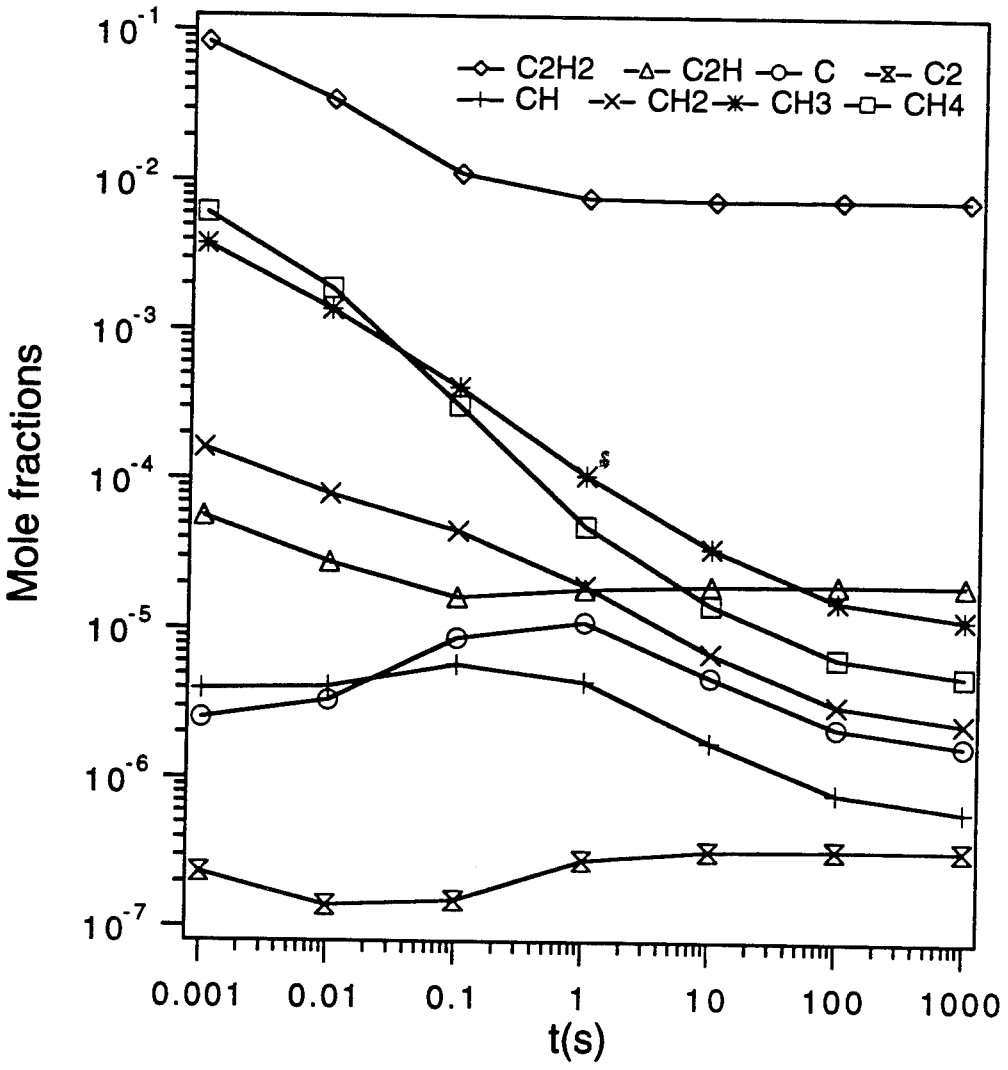

(c)

Fig. 6 — (Continues) Mole fractions of carbon-containing species at T=2500 K and inlet [EtOH]/[H_2O] ratio 1.1 at pressure equal to (a) 0.001 atm., (b) 0.01 atm., and (c) 0.1 atm.

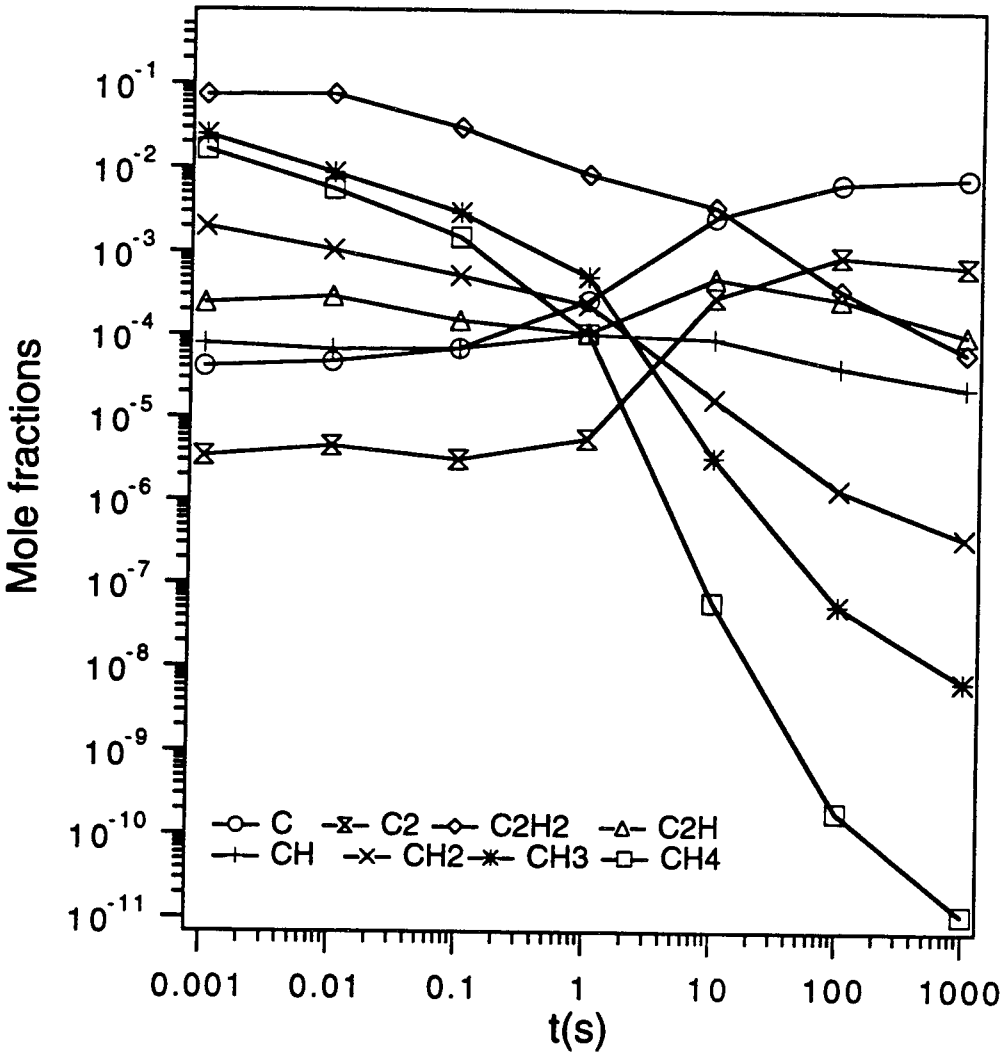

(a)

Fig. 7 — Mole fractions of carbon-containing species at T=3000 K and inlet [EtOH]/[H_2O] ratio 1.1 at pressure equal to (a) 0.001 atm., (b) 0.01 atm., and (c) 0.1 atm.

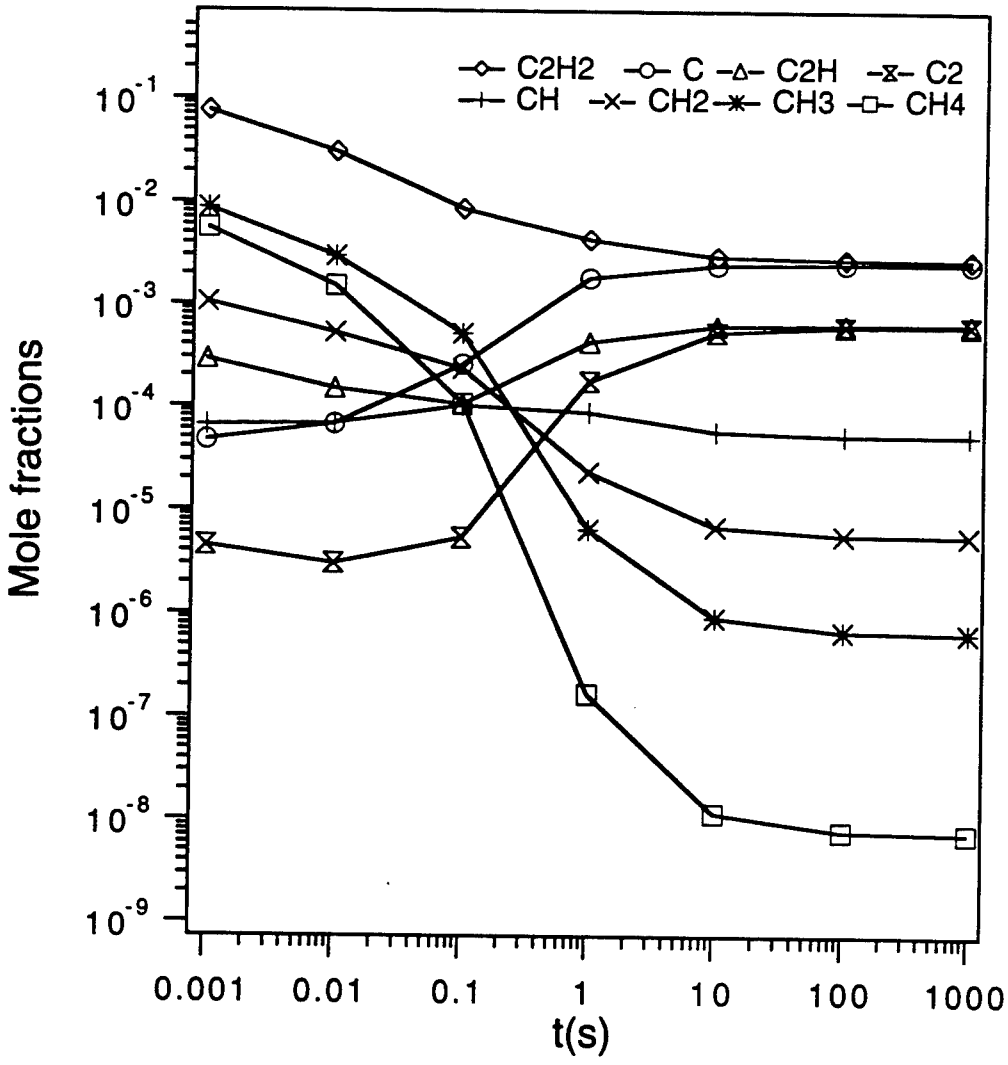

(b)

Fig. 7 — (Continues) Mole fractions of carbon-containing species at T=3000 K and inlet [EtOH]/[H_2O] ratio 1.1 at pressure equal to (a) 0.001 atm., (b) 0.01 atm., and (c) 0.1 atm.

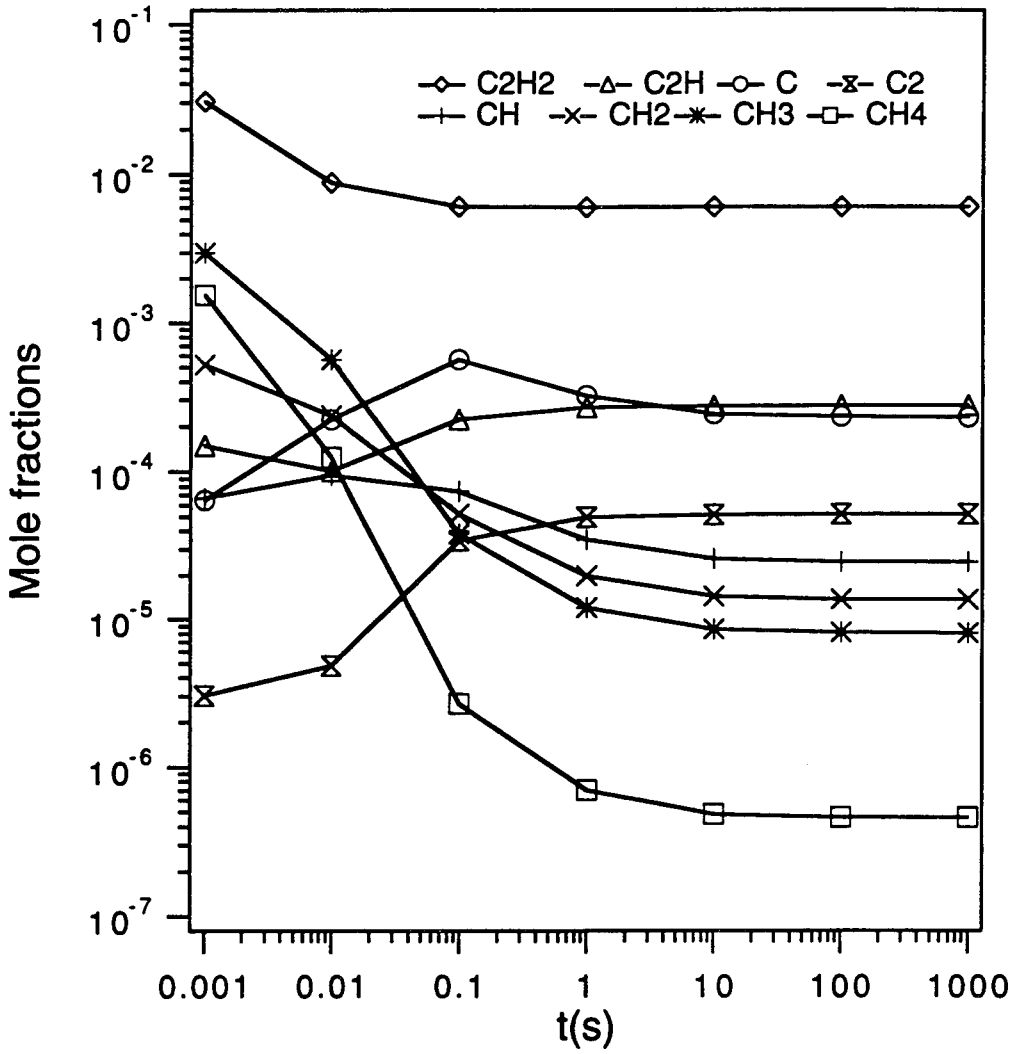

(c)

Fig. 7 — (Continues) Mole fractions of carbon-containing species at T=3000 K and inlet [EtOH]/[H_2O] ratio 1.1 at pressure equal to (a) 0.001 atm., (b) 0.01 atm., and (c) 0.1 atm.

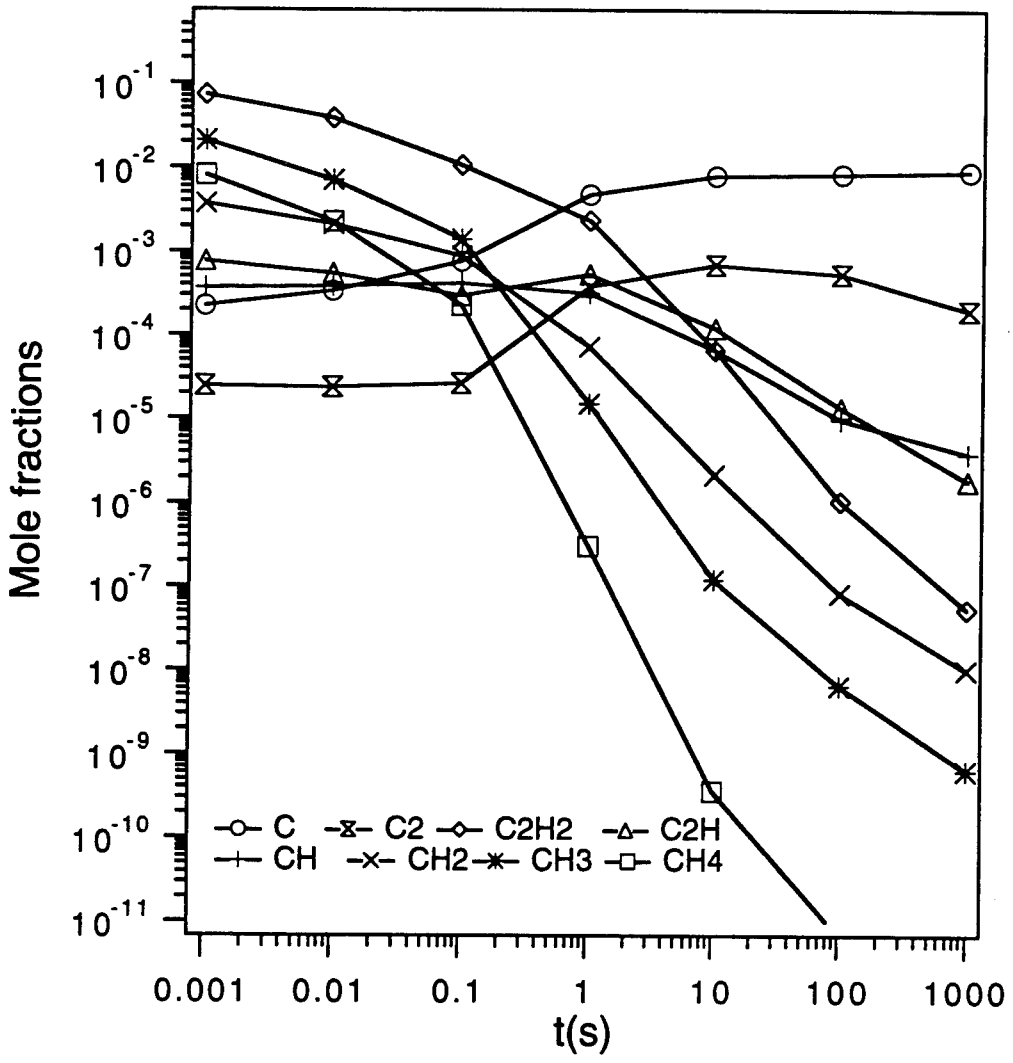

(a)

Fig. 8 — Mole fractions of carbon-containing species at T=3500 K and inlet [EtOH]/[H_2O] ratio 1.1 at pressure equal to (a) 0.001 atm., (b) 0.01 atm., and (c) 0.1 atm.

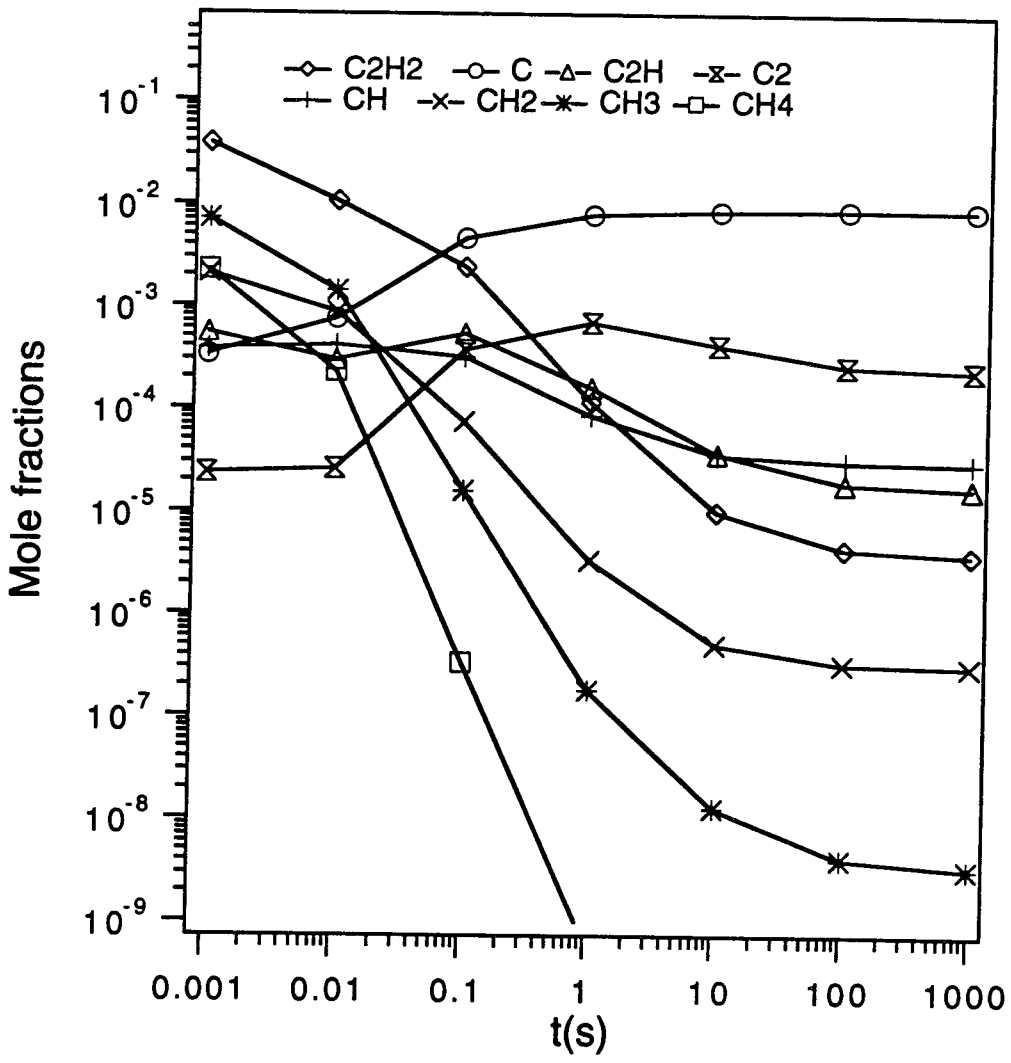

(b)

Fig. 8 — (Continues) Mole fractions of carbon-containing species at T=3500 K and inlet [EtOH]/[H_2O] ratio 1.1 at pressure equal to (a) 0.001 atm., (b) 0.01 atm., and (c) 0.1 atm.

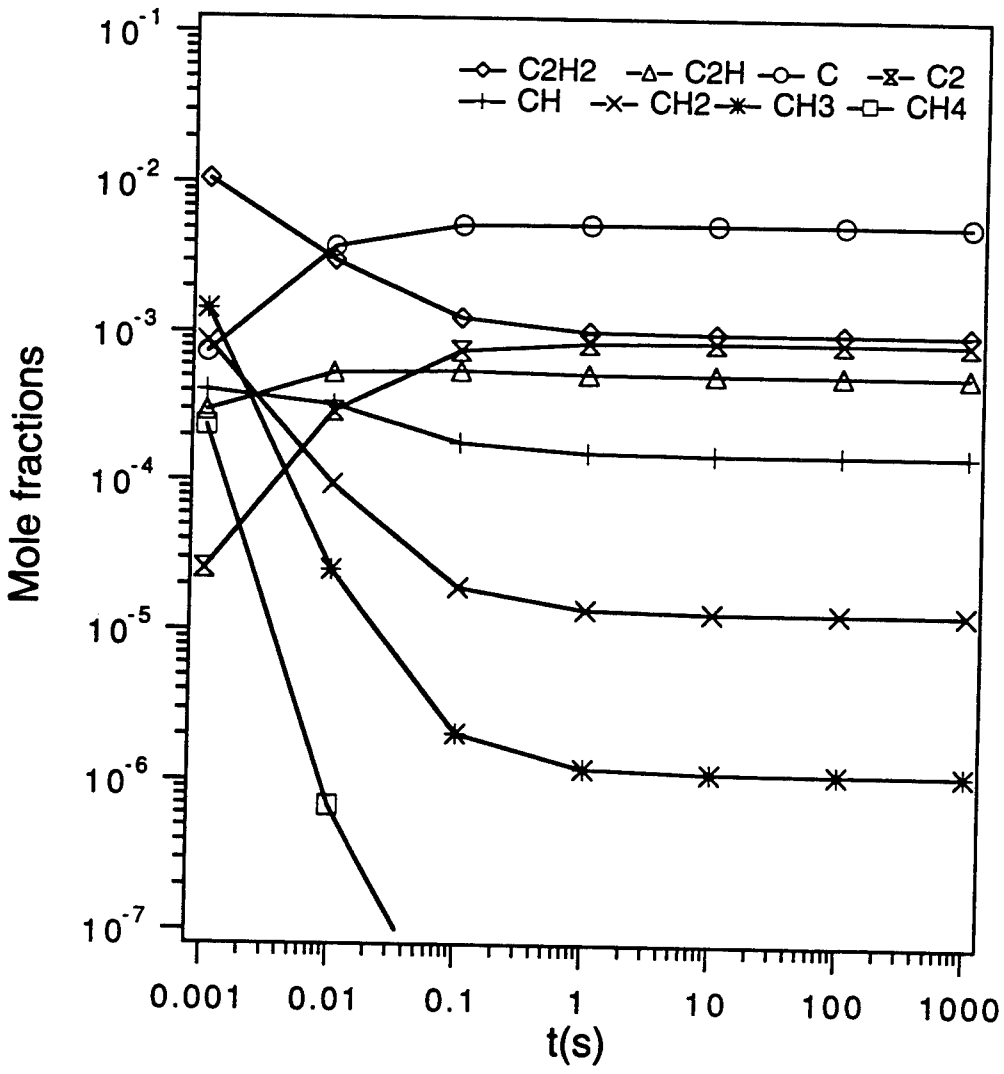

(c)

Fig. 8 — (Continues) Mole fractions of carbon-containing species at T=3500 K and inlet [EtOH]/[H_2O] ratio 1.1 at pressure equal to (a) 0.001 atm., (b) 0.01 atm., and (c) 0.1 atm.

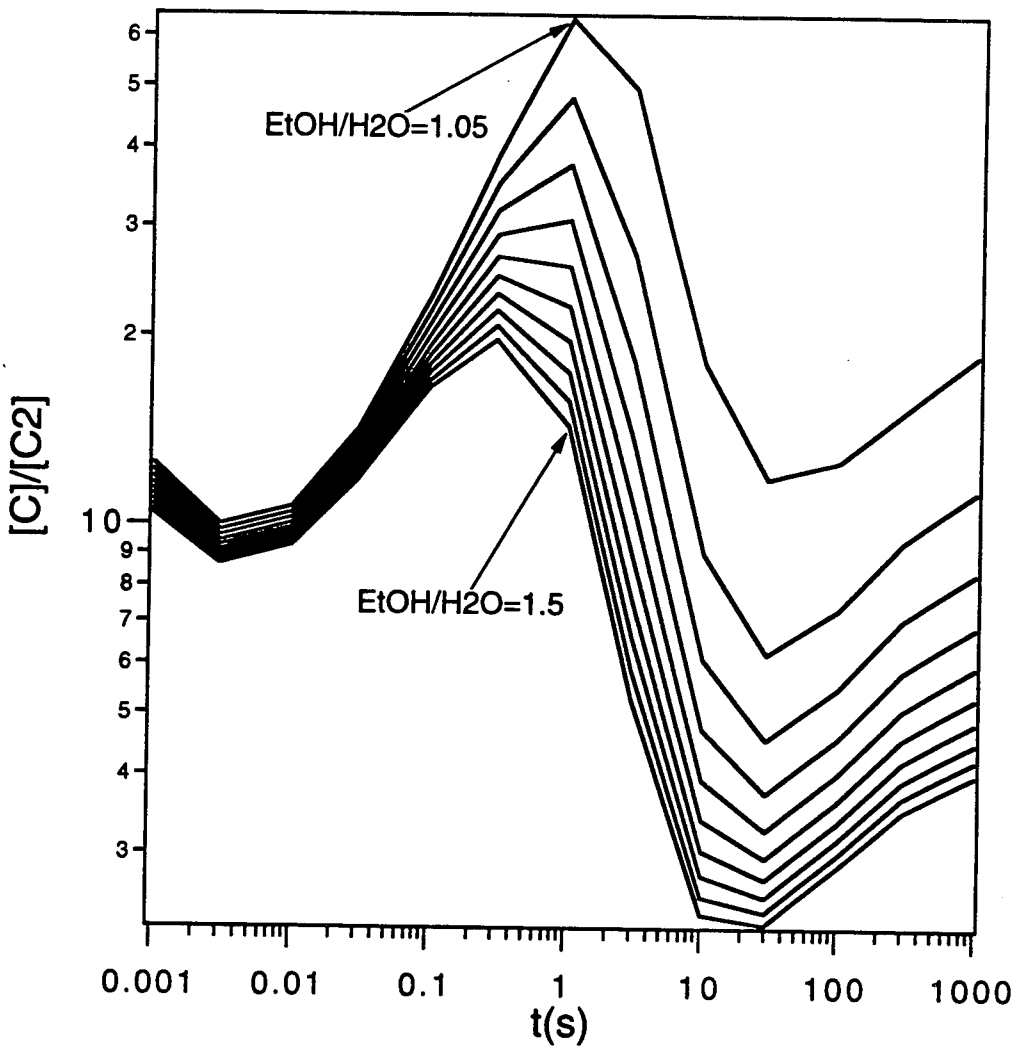

(a)

Fig. 9 — Ratios (a) [C]/[C_2], (b) [C]/[C_2H], and (c) [C]/[C_2H_2] as a function of inlet gas composition for T=3000 K and P=0.001 atm.

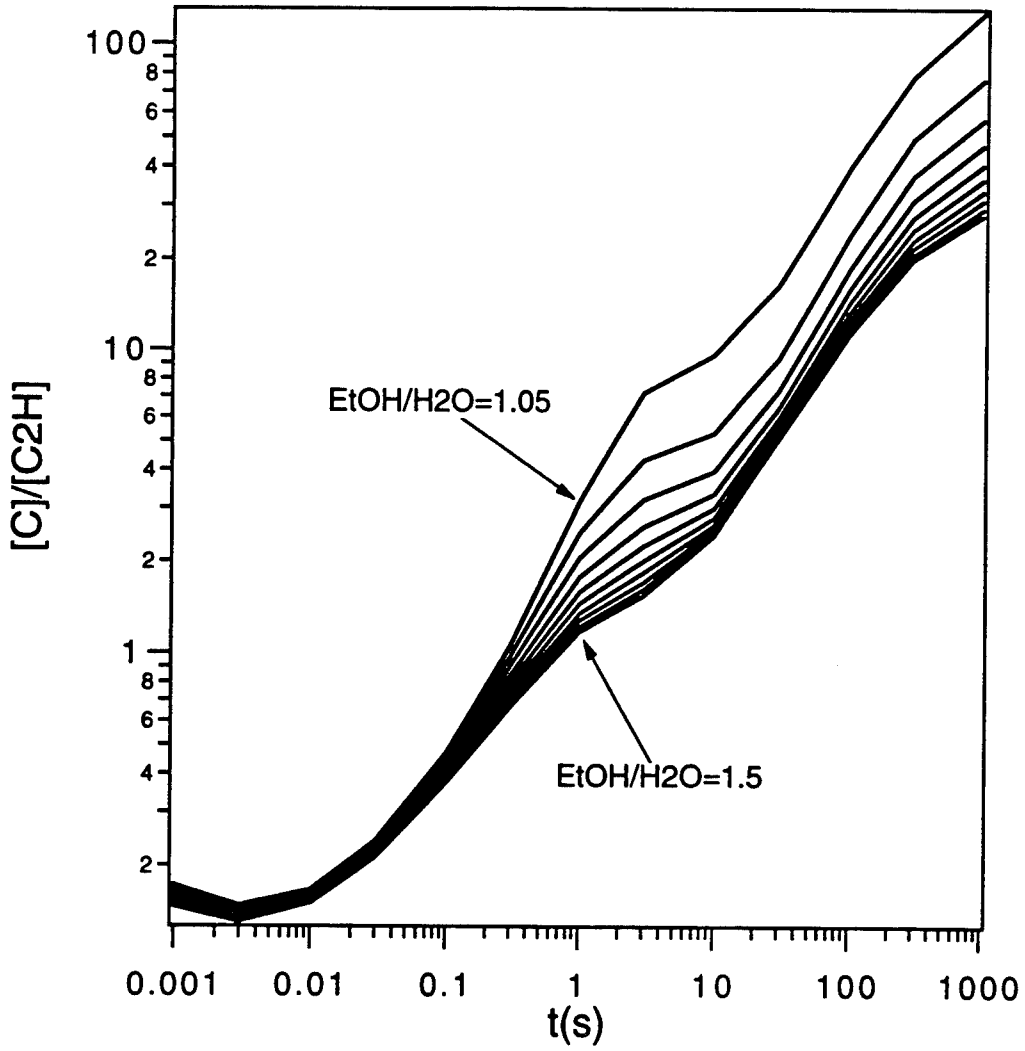

(b)

Fig. 9 — (Continues) Ratios (a) $[C]/[C_2]$, (b) $[C]/[C_2H]$, and (c) $[C]/[C_2H_2]$ as a function of inlet gas composition for T=3000 K and P=0.001 atm.

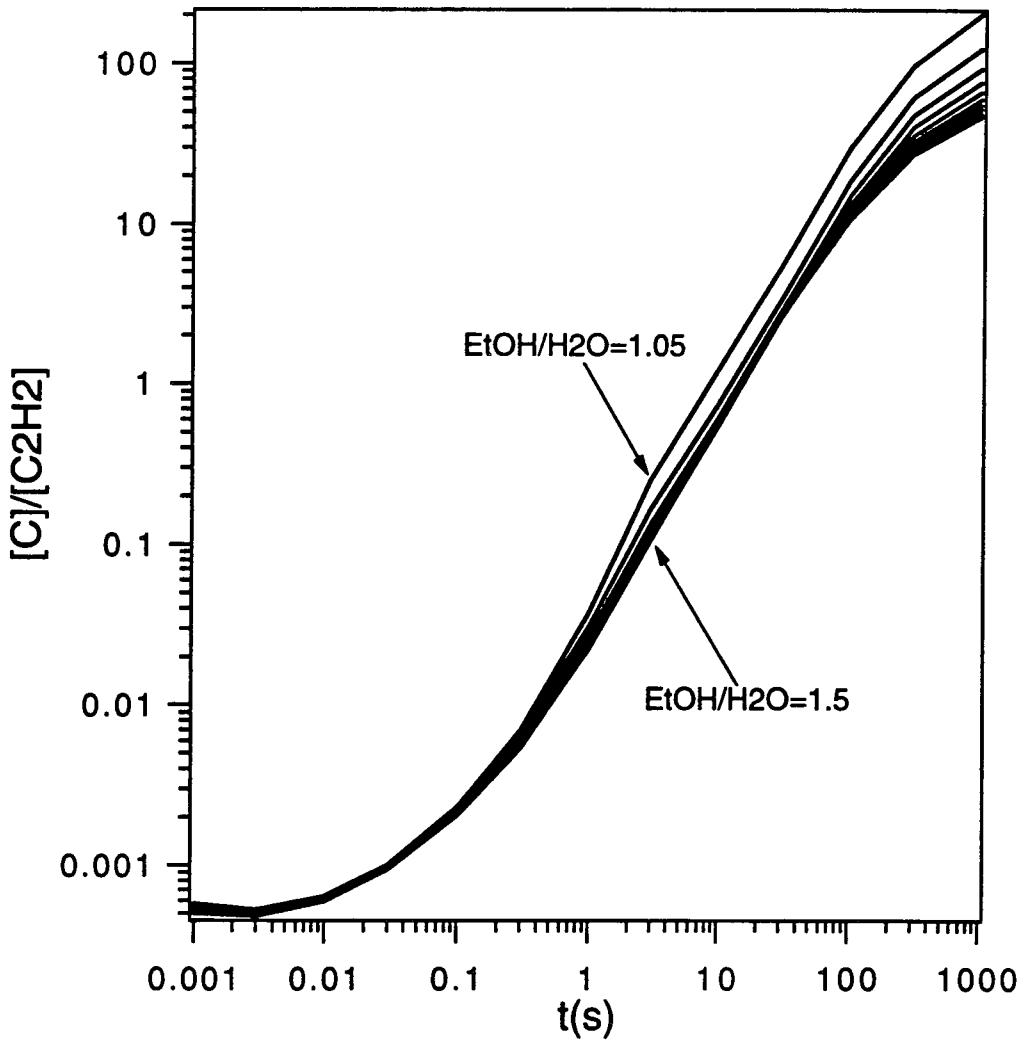

(c)

Fig. 9 — (Continues) Ratios (a) $[C]/[C_2]$, (b) $[C]/[C_2H]$, and (c) $[C]/[C_2H_2]$ as a function of inlet gas composition for T=3000 K and P=0.001 atm.